J Paleolimnol (2011) 46:423–452
DOI 10.1007/s10933-009-9346-3

ORIGINAL PAPER

Climate changes and human activities recorded in the sediments of Lake Estanya (NE Spain) during the Medieval Warm Period and Little Ice Age

Mario Morellón · Blas Valero-Garcés · Penélope González-Sampériz · Teresa Vegas-Vilarrúbia · Esther Rubio · Maria Rieradevall · Antonio Delgado-Huertas · Pilar Mata · Óscar Romero · Daniel R. Engstrom · Manuel López-Vicente · Ana Navas · Jesús Soto

Received: 5 January 2009 / Accepted: 11 May 2009 / Published online: 4 June 2009

Abstract A multi-proxy study of short sediment cores recovered in small, karstic Lake Estanya (42°02′ N, 0°32′ E, 670 m.a.s.l.) in the Pre-Pyrenean Ranges (NE Spain) provides a detailed record of the complex environmental, hydrological and anthropogenic interactions occurring in the area since medieval times. The integration of sedimentary facies, elemental and isotopic geochemistry, and biological proxies (diatoms, chironomids and pollen), together with a robust chronological control, provided by AMS radiocarbon dating and ^{210}Pb and ^{137}Cs radiometric techniques, enabled precise reconstruction of the main phases of environmental change, associated with the Medieval Warm Period (MWP), the Little Ice Age (LIA) and the industrial era. Shallow lake levels and saline conditions with poor development of littoral environments prevailed during medieval times (1150–1300 AD). Generally higher water levels and

Jesús Soto—deceased.

M. Morellón (✉) · B. Valero-Garcés · P. González-Sampériz
Departamento de Procesos Geoambientales y Cambio Global, Instituto Pirenaico de Ecología (IPE)—CSIC, Campus de Aula Dei. Avda Montañana 1005, 50059 Zaragoza, Spain
e-mail: mariomm@ipe.csic.es

T. Vegas-Vilarrúbia · E. Rubio · M. Rieradevall
Departament d'Ecologia, Facultat de Biologia, Universitat de Barcelona, Av. Diagonal 645, Edf. Ramón Margalef, 08028 Barcelona, Spain

A. Delgado-Huertas
Estación Experimental del Zaidín (EEZ)—CSIC, Prof. Albareda 1, 18008 Granada, Spain

P. Mata
Facultad de Ciencias del Mar y Ambientales, Universidad de Cádiz, Polígono Río San Pedro s/n, 11510 Puerto Real (Cádiz), Spain

Ó. Romero
Facultad de Ciencias, Instituto Andaluz de Ciencias de la Tierra (IACT)—CSIC, Universidad de Granada, Campus Fuentenueva, 18002 Granada, Spain

D. R. Engstrom
St. Croix Watershed Research Station, Science Museum of Minnesota, Marine on St. Croix, MN 55047, USA

M. López-Vicente · A. Navas
Departamento de Suelo y Agua, Estación Experimental de Aula Dei (EEAD)—CSIC, Campus de Aula Dei, Avda. Montañana 1005, 50059 Zaragoza, Spain

J. Soto
Departamento de Ciencias Médicas y Quirúrgicas, Facultad de Medicina, Universidad de Cantabria Avda. Herrera Oria s/n, 39011 Santander, Spain

more dilute waters occurred during the LIA (1300–1850 AD), although this period shows a complex internal paleohydrological structure and is contemporaneous with a gradual increase of farming activity. Maximum lake levels and flooding of the current littoral shelf occurred during the nineteenth century, coinciding with the maximum expansion of agriculture in the area and prior to the last cold phase of the LIA. Finally, declining lake levels during the twentieth century, coinciding with a decrease in human pressure, are associated with warmer climate conditions. A strong link with solar irradiance is suggested by the coherence between periods of more positive water balance and phases of reduced solar activity. Changes in winter precipitation and dominance of NAO negative phases would be responsible for wet LIA conditions in western Mediterranean regions. The main environmental stages recorded in Lake Estanya are consistent with Western Mediterranean continental records, and show similarities with both Central and NE Iberian reconstructions, reflecting a strong climatic control of the hydrological and anthropogenic changes during the last 800 years.

Keywords Lake Estanya · Iberian Peninsula · Western Mediterranean · Medieval Warm Period · Little Ice Age · Twentieth century · Human impact

Introduction

In the context of present-day global warming, there is increased interest in documenting climate variability during the last millennium (Jansen et al. 2007). It is crucial to reconstruct pre-industrial conditions to discriminate anthropogenic components (i.e. greenhouse gases, land-use changes) from natural forcings (i.e. solar variability, volcanic emissions) of current warming. The timing and structure of global thermal fluctuations which occurred during the last millennium is a well-established theme in paleoclimate research. A period of relatively high temperatures during the Middle Ages (Medieval Warm Period—MWP; Bradley et al. 2003) was followed by several centuries of colder temperatures (Fischer et al. 1998) and mountain glacier readvances (Wanner et al. 2008) (Little Ice Age - LIA), and an abrupt increase in temperatures contemporaneous with industrialization during the last century (Mann et al. 1999). These climate fluctuations were accompanied by strong hydrological and environmental impacts (Mann and Jones 2003; Osborn and Briffa 2006; Verschuren et al. 2000a), but at a regional scale (e.g. the western Mediterranean), we still do not know the exact temporal and spatial patterns of climatic variability during those periods. They have been related to variations in solar activity (Bard and Frank 2006) and the North Atlantic Oscillation (NAO) index (Kirov and Georgieva 2002; Shindell et al. 2001), although both linkages remain controversial. More records are required to evaluate the hydrological impact of these changes, their timing and amplitude, in temperate continental areas (Luterbacher et al. 2005).

Lake sediments have long been used to reconstruct environmental changes driven by climate fluctuations (Cohen 2003; Last and Smol 2001). In the Iberian Peninsula, numerous lake studies document a large variability during the last millennium: Lake Estanya (Morellón et al. 2008; Riera et al. 2004), Tablas de Daimiel (Gil García et al. 2007), Sanabria (Luque and Julià 2002), Doñana (Sousa and García-Murillo 2003), Archidona (Luque et al. 2004), Chiprana (Valero-Garcés et al. 2000), Zoñar (Martín-Puertas et al. 2008; Valero-Garcés et al. 2006), and Taravilla (Moreno et al. 2008; Valero Garcés et al. 2008). However, most of these studies lack the chronological resolution to resolve the internal, sub-centennial structure of the main climatic phases (MWP, LIA).

In Mediterranean areas, such as the Iberian Peninsula, characterized by an annual water deficit and a long history of human activity, lake hydrology and sedimentary dynamics at certain sites could be controlled by anthropogenic factors [e.g. Lake Chiprana (Valero-Garcés et al. 2000); Tablas de Daimiel (Domínguez-Castro et al. 2006)]. The interplay between climate changes and human activities and the relative importance of their roles in sedimentation strongly varies through time, and it is often difficult to ascribe limnological changes to one of these two forcing factors (Brenner et al. 1999; Cohen 2003; Engstrom et al. 2006; Smol 1995; Valero-Garcés et al. 2000; Wolfe et al. 2001). Nevertheless, in spite of intense human activity, lacustrine records spanning the last centuries have documented changes in vegetation and flood frequency (Moreno et al. 2008), water chemistry (Romero-Viana et al. 2008)

and sedimentary regime (Martín-Puertas et al. 2008), mostly in response to regional moisture variability associated with recent climatic fluctuations.

This paper evaluates the recent (last 800 years) palaeoenvironmental evolution of Lake Estanya (NE Spain), a relatively small (18.9 ha), deep (z_{max} 20 m), groundwater-fed, karstic lake located in the transitional area between the humid Pyrenees and the semi-arid Central Ebro Basin. Lake Estanya water level has responded rapidly to recent climate variability during the late twentieth century (Morellón et al. 2008) and the >21-ka sediment sequence reflects its hydrological variability at centennial and millennial scales since the LGM (Morellón et al. 2009). The evolution of the lake during the last two millennia has been previously studied in a littoral core (Riera et al. 2004, 2006). The area has a relatively long history of human occupation, agricultural practices and water management (Riera et al. 2004), with increasing population during medieval times, a maximum in the nineteenth century, and a continuous depopulation trend during the twentieth century. Here we present a study of short sediment cores from the distal areas of the lake, analyzed with a multi-proxy strategy, including sedimentological, geochemical and biological variables. The combined use of ^{137}Cs, ^{210}Pb and AMS ^{14}C provides excellent chronological control and resolution.

Regional setting

Geological and geomorphological setting

The Estanya Lakes (42°02′N, 0°32′E; 670 m. a.s.l.) constitute a karstic system located in the Southern Pre-Pyrenees, close to the northern boundary of the Ebro River Basin, in north-eastern Spain (Fig. 1c). Karstification processes affecting Upper Triassic carbonate and evaporite formations have favoured the extensive development of large *poljes* and dolines in the area (IGME 1982; Sancho-Marcén 1988). The Estanya lakes complex has a relatively small endorheic basin of 2.45 km^2 (López-Vicente et al. 2009) and consists of three dolines: the 7-m deep 'Estanque Grande de Arriba', the seasonally flooded 'Estanque Pequeño de Abajo' and the largest and deepest 'Estanque Grande de Abajo' on which this research focuses (Fig. 1a). Lake basin substrate is constituted by Upper Triassic, low-permeability marls and claystones (Keuper facies), whereas Middle Triassic limestone and dolostone Muschelkalk facies occupy the highest elevations of the catchment (Sancho-Marcén 1988; Fig. 1a).

Lake hydrology and limnology

The main lake, 'Estanque Grande de Abajo' has a relatively small catchment of 106.5 ha (López-Vicente et al. 2009), and comprises two sub-basins with steep margins and maximum water depths of 12 and 20 m, separated by a sill, 2–3 m below present-day lake level (Fig. 1a). Although there is neither a permanent inlet nor outlet, several ephemeral creeks drain the catchment (Fig. 1a; López-Vicente et al. 2009). The lakes are mainly fed by groundwaters from the surrounding local limestone and dolostone aquifer, which also feeds a permanent spring (0.3 l/s), located at the north end of the catchment (Fig. 1a). Estimated evapotranspiration is 774 mm, exceeding rainfall (470 mm) by about 300 mm year^{-1}. Hydrological balance is controlled by groundwater inputs, via subaqueous springs, and evaporation output (Morellón et al. (2008) and references therein). A twelfth century canal system connected the three dolines and provided water to the largest and topographically lowest one, the 'Estanque Grande de Abajo' (Riera et al. 2004). However, these canals no longer function and thus, lake level is no longer human-controlled.

Lake water is brackish and oligotrophic. Its chemical composition is dominated by sulphate and calcium ($[SO_4^{2-}] > [Ca^{2+}] > [Mg^{2+}] > [Na^{+}]$). The high electrical conductivity in the epilimnion (3,200 µS cm^{-1}) compared to water chemistry of the nearby spring (630 µS cm^{-1}) suggests a long residence time and strong influence of evaporation in the system, as indicated by previous studies (Villa and Gracia 2004). The lake is monomictic, with thermal stratification and anoxic hypolimnetic conditions from March to September, as shown by early (Ávila et al. 1984) and recent field surveys (Morellón et al. 2009).

Climate and vegetation

The region is characterized by Mediterranean continental climate, with a long summer drought (León-Llamazares 1991). Mean annual temperature is 14°C and ranges from 4°C (January) to 24°C (July) (Morellón et al. (2008) and references therein). Lake

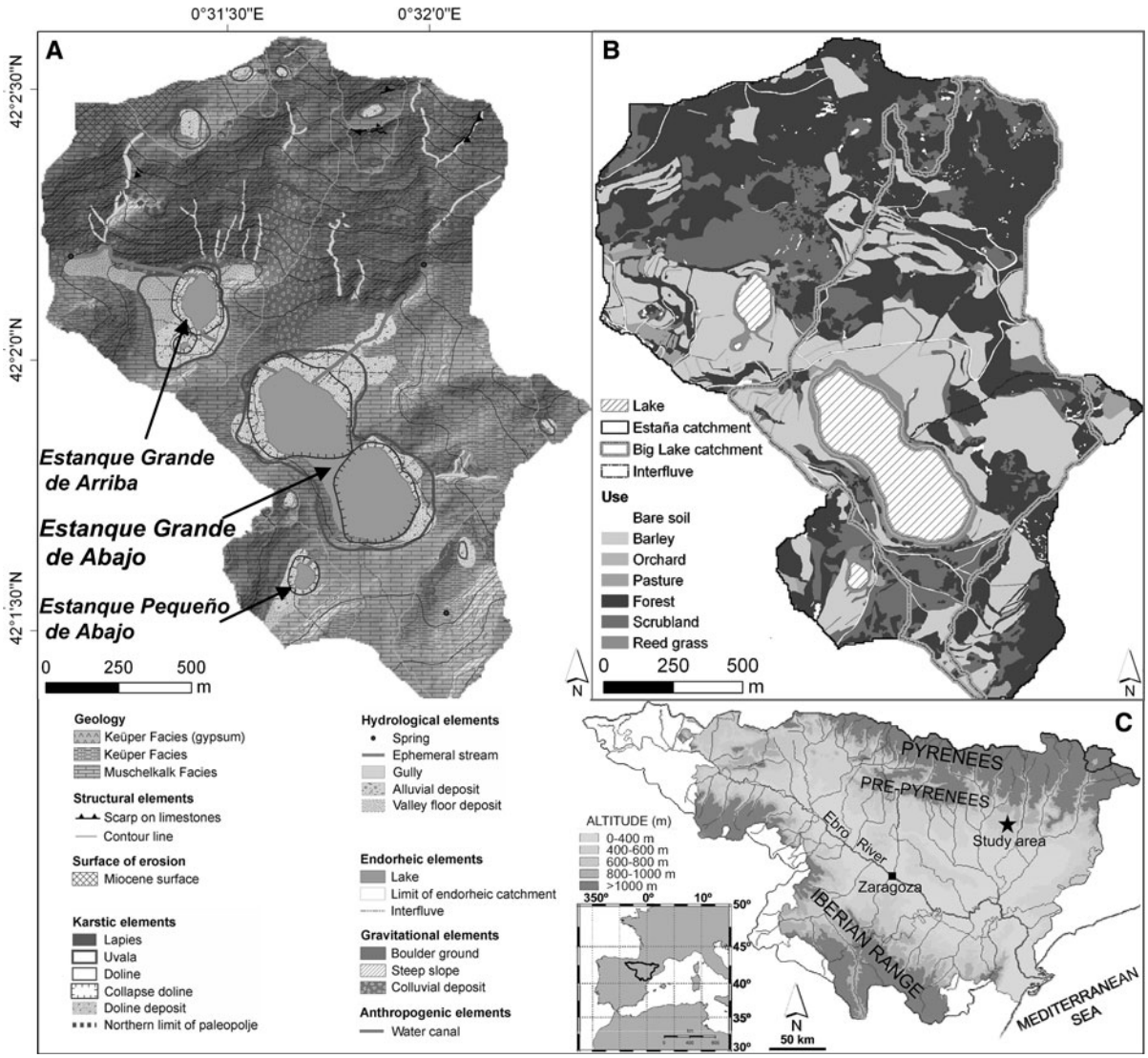

Fig. 1 **a** Geomorphological map of the 'Estanya lakes' karstic system. **b** Land use map of the watershed. [Modified from (López-Vicente et al. 2009)]. **c** Location of the study area marked by a star in the Ebro River watershed

Estanya is located at the transitional zone between Mediterranean and Submediterranean bioclimatic regimes (Rivas-Martínez 1982), at 670 m.a.s.l. The Mediterranean community is a sclerophyllous woodland dominated by evergreen oak, whereas the Submediterranean is dominated by drought-resistant deciduous oaks (Peinado Lorca and Rivas-Martínez 1987). Present-day landscape is a mosaic of natural vegetation with patches of cereal crops. The catchment lowlands and plain areas, more suitable for farming, are mostly dedicated to barley cultivation, with small orchards located close to creeks. Higher elevation areas are mostly occupied by scrublands and oak forests, more developed on northfacing slopes. The lakes are surrounded by a wide littoral belt of hygrophyte communities of *Phragmites* sp., *Juncus* sp., *Typha* sp., and *Scirpus* sp. (Fig. 1b).

Methods

The Lake Estanya watershed was delineated and mapped using the available topographic and geological maps and aerial photographs. Coring operations

were conducted in two phases: four modified Kullenberg piston cores (1A-1K to 4A-1K) and four short gravity cores (1A-1M to 4A-1M) were retrieved in 2004 using coring equipment and a platform from the Limnological Research Center (LRC), University of Minnesota; an additional Uwitec© core (5A-1U) was recovered in 2006. Short cores 1A-1M and 4A-1M were sub-sampled in the field every 1 cm for ^{137}Cs and ^{210}Pb dating. The uppermost 146 and 232 cm of long cores 1A-1 K and 5A-1U, respectively, were selected and sampled for different analyses. The sediment/water interface was not preserved in Kullenberg core 1A, and the uppermost part of the sequence was reconstructed using a parallel short core (1A-1 M).

Before splitting the cores, physical properties were measured by a Geotek Multi-Sensor Core Logger (MSCL) every 1 cm. The cores were subsequently imaged with a DMT Core Scanner and a GEOSCAN II digital camera. Sedimentary facies were defined by visual macroscopic description and microscopic observation of smear slides following LRC procedures (Schnurrenberger et al. 2003) and by mineralogical, organic and geochemical compositions. The 5A-1U core archive halves were measured at 5-mm resolution for major, light elements (Al, Si, P, S, K, Ca, Ti, Mn and Fe) using a AVAATECH XRF II core scanner. The measurements were produced using an X-ray current of 0.5 mA at 60 s count time and 10 kV X-ray voltage to obtain statistically significant values. Following common procedures (Richter et al. 2006), the results obtained by the XRF core scanner are expressed as element intensities. Statistical multivariate analysis of XRF data was carried out with SPSS 14.0.

Samples for Total Organic Carbon (TOC) and Total Inorganic Carbon (TIC) were taken every 2 cm in all the cores. Cores 1A-1 K and 1A-1M were additionally sampled every 2 cm for Total Nitrogen (TN), every 5 cm for mineralogy, stable isotopes, element geochemistry, biogenic silica (BSi) and diatoms; and every 10 cm for pollen and chironomids. Sampling resolution in core 1A-1M was modified depending on sediment availability. TOC and TIC were measured with a LECO SC144 DR furnace. TN was measured by a VARIO MAX CN elemental analyzer. Whole-sediment mineralogy was characterized by X-ray diffraction with a Philips PW1820 diffractometer and the relative mineral abundance was determined using peak intensity following the procedures described in Chung (1974a, b).

Isotope measurements were carried out on water and bulk sediment samples using conventional mass spectrometry techniques with a Delta Plus XL or Delta XP mass spectrometer (IRMS). Carbon dioxide was obtained from the carbonates using 100% phosphoric acid for 12 h in a thermostatic bath at 25°C (McCrea 1950). After carbonate removal by acidification with HCl 1:1, $\delta^{13}C_{org}$ was measured by an Elemental Analyzer Fison NA1500 NC. Water was analyzed using the CO_2–H_2O equilibration method (Cohn and Urey 1938; Epstein and Mayeda 1953). In all the cases, analytical precision was better than 0.1‰. Isotopic values are reported in the conventional delta notation relative to the VPDB (organic matter and carbonates) and SMOW (water) standards.

Biogenic silica content was analyzed following automated leaching (Müller and Schneider 1993) by alkaline extraction (De Master 1981). Diatoms were extracted from dry sediment samples of 0.1 g and prepared using H_2O_2 for oxidation, and HCl and sodium pyrophosphate to remove carbonates and clays, respectively. Specimens were mounted in Naphrax and analyzed with a Polyvar light microscope at 1,250× magnification. Valve concentrations per unit weight of sediment were calculated using plastic microspheres (Battarbee 1986) and also expressed as relative abundances (%) of each taxon. At least 300 valves were counted in each sample; when diatom content was lower, counting continued until reaching 1,000 microspheres (Abrantes et al. 2005; Battarbee et al. 2001; Flower 1993). Taxonomic identifications were made using specialized literature (Aboal et al. 2003; Krammer 2002; Krammer and Lange-Bertalot 1986; Lange-Bertalot 2001; Witkowski et al. 2000; Wunsam et al. 1995).

Chironomid head capsules (HC) were extracted from samples of 4–10 g of sediment. Samples were deflocculated in 10% KOH, heated to 70°C and stirred at 300 rpm for 20 min. After sieving, the >90 μm fraction was poured in small quantities into a Bolgorov tray and examined under a stereo microscope. HC were picked out manually, dehydrated in 96% ethanol and up to four HC were slide mounted in Euparal on a single cover glass, ventral side upwards. The larval HC were identified to the lowest taxonomic level using *ad hoc* literature (Brooks et al. 2007; Rieradevall and Brooks 2001; Schmid 1993; Wiederholm 1983). Fossil densities (individuals per g fresh weight), species richness,

and relative abundances (%) of each taxon were calculated.

Pollen grains were extracted from ~2 g samples of sediment, using the classic chemical method (Moore et al. 1991), modified according to Dupré (1992) and using Thoulet heavy liquid (2.0 density). *Lycopodium clavatum* tablets were added to calculate pollen concentrations (Stockmarr 1971). The pollen sum does not include the hygrohydrophytes group and fern spores. A minimum of 200–250 terrestrial pollen grains was counted in all samples, and 71 taxa were identified. Diagrams of diatoms, chironomids and pollen were constructed using Psimpoll software (Bennet 2002).

The chronology for the lake sediment sequence was developed using three Accelerator Mass Spectrometry (AMS) ^{14}C dates from core 1A-1K, analyzed at the Poznan Radiocarbon Laboratory (Poland), and ^{137}Cs and ^{210}Pb dates in short cores 1A-1M and 2A-1M, obtained by gamma ray spectrometry. Excess (unsupported) ^{210}Pb was calculated in 1A-1M by the difference between total ^{210}Pb and ^{214}Pb for individual core intervals. In core 2A-1M, where ^{214}Pb was not measured, excess ^{210}Pb in each level was calculated as the difference between total ^{210}Pb in each level and an estimate of supported ^{210}Pb, which was the average ^{210}Pb activity in the lowermost seven core intervals, below 24 cm. Lead-210 dates were determined using the constant rate of supply (CRS) model (Appleby 2001). Radiocarbon dates were converted into calendar years AD with CALPAL_A software (Weninger and Jöris 2004) using the calibration curve INTCAL 04 (Reimer et al. 2004), selecting the median of the 95.4% distribution (2σ probability interval).

Results

Core correlation and chronology

The 161-cm-long composite sequence from the offshore, distal area of Lake Estanya was constructed using Kullenberg core 1A-1K, and completed by adding the uppermost 15 cm of short core 1A-1M (Fig. 2b). The entire sequence was also recovered in the top section (232 cm long) of core 5A-1U, retrieved with a Uwitec coring system. These sediments correspond to the upper clastic unit I defined for the entire sequence of Lake Estanya (Morellón et al. 2008, 2009). Thick clastic sediment unit I was deposited continuously throughout the whole lake basin, as indicated by seismic data, marking the most significant transgressive episode during the late Holocene (Morellón et al. 2009). Correlation between all the cores was based on lithology, TIC and TOC core logs (Fig. 2a). Given the short distance between coring sites 1A and 5A, differences in sediment thickness are attributed to the differential degree of compression caused by the two coring systems, rather than to variable sedimentation rates.

Total ^{210}Pb activities in cores 1A-1M and 2A-1M are relatively low, with near-surface values of 9 pCi/g in 1A-1M (Fig. 3a) and 6 pCi/g in 2A-1M (Fig. 3b). Supported ^{210}Pb (^{214}Pb) ranges between 2 and 4 pCi/g in 1A-1M and is estimated at 1.22 ± 0.09 pCi/g in 2A-1M (Fig. 3a, b). Constant rate of supply (CRS) modelling of the ^{210}Pb profiles gives a lowermost date of ca. 1850 AD (±36 years) at 27 cm in 1A-1 M (Fig. 3c, e) and a similar date at 24 cm in 2A-1M (Fig. 3d, f). The ^{210}Pb chronology for core 1A-1M also matches closely ages for the profile derived using ^{137}Cs. Well-defined ^{137}Cs peaks at 14–15 cm and 8–9 cm, are bracketed by ^{210}Pb dates of 1960–1964 AD and 1986–1990 AD, respectively, and correspond to the 1963 maximum in atmospheric nuclear bomb testing and a secondary deposition event likely from the 1986 Chernobyl nuclear accident (Fig. 3c). The sediment accumulation rate obtained by ^{210}Pb and ^{137}Cs chronologies is consistent with the linear sedimentation rate for the upper 60 cm derived from radiocarbon dates (Fig. 3 g). Sediment accumulation profiles for both sub-basins are similar and display an increasing trend from 1850 AD until late 1950 AD, a sharp decrease during 1960–1980 AD, and an increase during the last decade (Fig. 3e, f).

The radiocarbon chronology of core 1A-1K is based on three AMS ^{14}C dates, all obtained from terrestrial plant macrofossil remains (Table 1). The age model for the composite sequence constituted by cores 1A-1M (15 uppermost cm) and core 1A-1K (146 cm), was constructed by linear interpolation using the 1986 and 1963 AD ^{137}Cs peaks (core 1A-1M) and the three AMS calibrated radiocarbon dates (1A-1K) (Fig. 3 g). The 161-cm-long composite sequence spans the last 860 years. To obtain a chronological model for parallel core 5A-1U, the ^{137}Cs peaks and the three calibrated radiocarbon

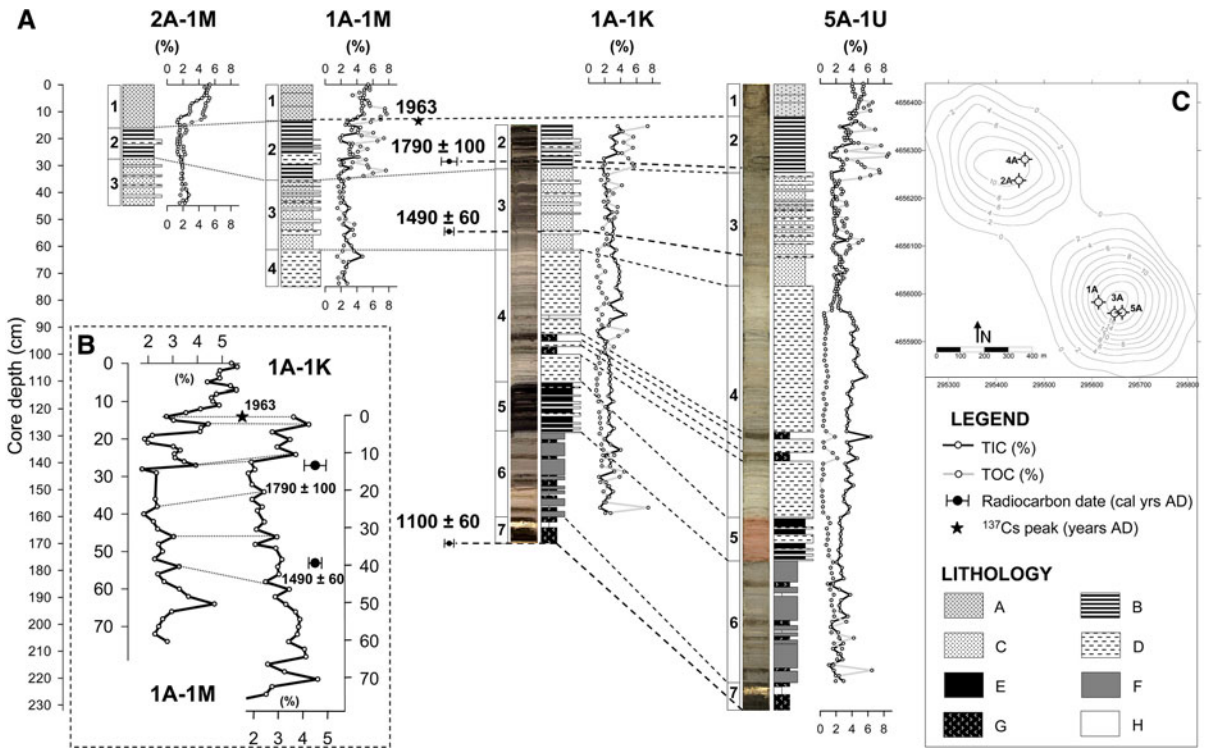

Fig. 2 **a** Correlation panel of cores 4A-1M, 1A-1M, 1A-1K and 5A-1U. Available core images, detailed sedimentological profiles and TIC and TOC core logs were used for correlation. AMS ^{14}C calibrated dates (years AD) from core 1A-1 K and 1963 AD ^{137}Cs maximum peak detected in core 1A-1 M are also indicated. Dotted lines represent lithologic correlation lines, whereas dashed lines correspond to correlation lines of sedimentary units' limits and other key beds used as tie points for the construction of the age model in core 5A-1U. See Table 2 for lithological descriptions. **b** Detail of correlation between cores 1A-1M and 1A-1K based on TIC percentages. **c** Bathymetric map of Lake Estanya with coring sites

dates were projected onto this core using detailed sedimentological profiles and TIC and TOC logs for core correlation (Fig. 2a). Ages for sediment unit boundaries and levels such as facies F intercalations within unit 4 (~93 and ~97 cm in core 1A-1K) (dashed correlation lines marked in Fig. 2a), were calculated for core 5A (Fig. 3g, h) using linear interpolation, as for core 1A-1K (Fig. 3h). The linear sedimentation rates (LSR) are lower in units 2 and 3 (0.87 mm/year) and higher in top unit 1 (3.41 mm/year) and bottom units 4–7 (3.94 mm/year).

The sediment sequence

Using detailed sedimentological descriptions, smear-slide microscopic observations, and compositional analyses, we defined eight facies in the studied sediment cores (Table 2). Sediment facies can be grouped into two main categories: (1) fine-grained, silt-to-clay-size sediments of variable texture (massive to finely laminated) (facies A, B, C, D, E and F), and (2) gypsum and organic-rich sediments composed of massive to barely laminated organic layers with intercalations of gypsum laminae and nodules (facies G and H). The first group of facies is interpreted as clastic deposition of material derived from the watershed (weathering and erosion of soils and bedrock, remobilization of sediment accumulated in valleys) and from littoral areas, and variable amounts of endogenic carbonates and organic matter. Organic and gypsum-rich facies occurred during periods of shallower and more chemically concentrated water conditions when algal and chemical deposition dominated. Interpretation of depositional subenvironments corresponding to each of the eight sedimentary facies enables reconstruction of depositional and hydrological changes in the Lake Estanya basin (Fig. 4; Table 2).

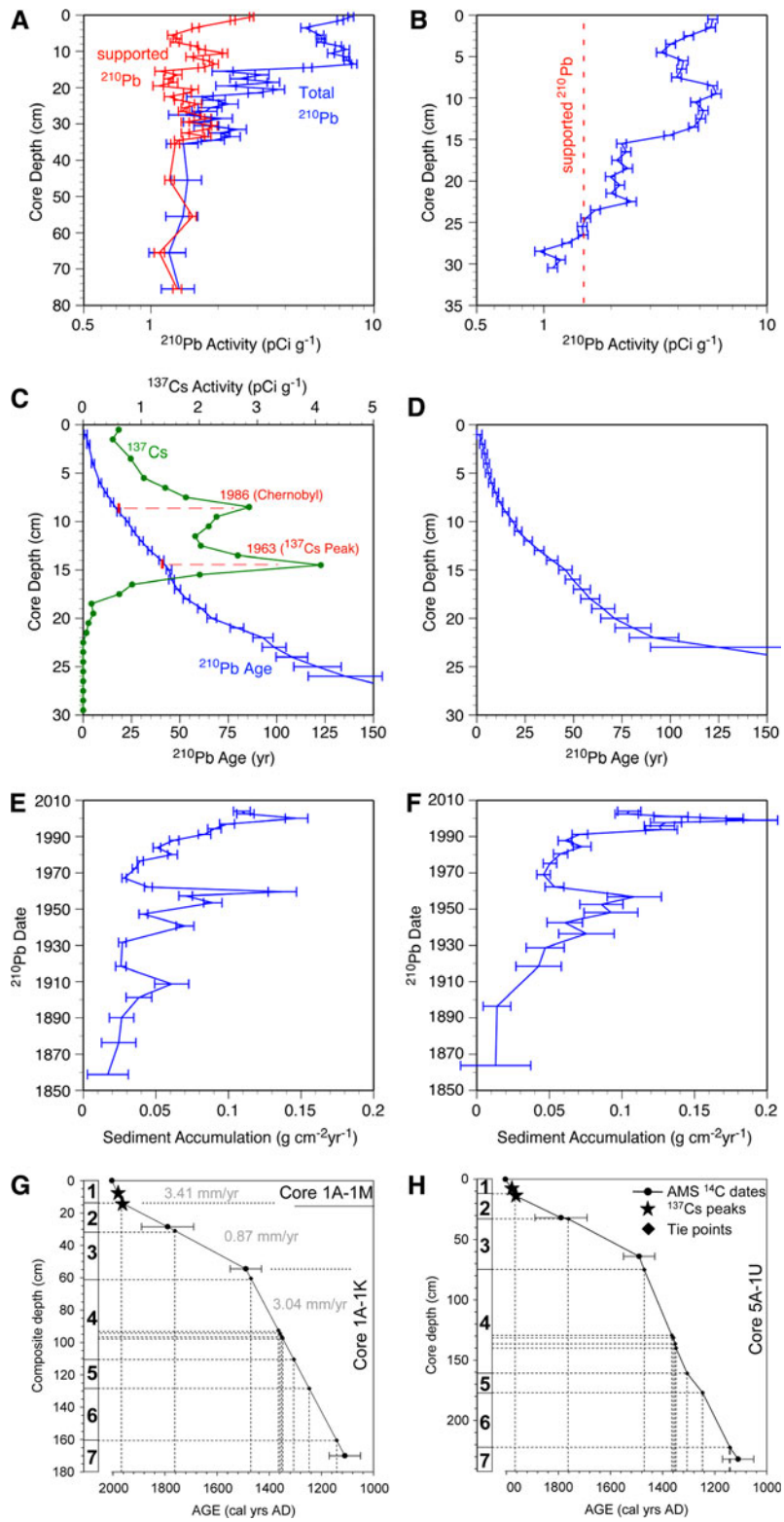

Fig. 3 Chronological framework of the studied Lake Estanya sequence. **a** Total ^{210}Pb activities of supported (*red*) and unsupported (*blue*) lead for core 1A-1M; **b** Total ^{210}Pb activities of supported (*red*) and unsupported (*blue*) lead for core 2A-1M; **c** Constant rate of supply modeling of ^{210}Pb values for core 1A-1M and ^{137}Cs profile for core 1A-1M, with maxima peaks of 1963 AD and 1986 are also indicated; **d** Constant rate of supply modeling of ^{210}Pb values for core 2A-1M; **e** ^{210}Pb based sediment accumulation rate for core 1A-1M; **f** ^{210}Pb based sediment accumulation rate for core 2A-1M; **g** Age model for the composite sequence of cores 1A-1M and 1A-1K obtained by linear interpolation of ^{137}Cs peaks and AMS radiocarbon dates. Tie points used to correlate to core 5A-1U are also indicated. **h** Age model for core 5A-1U generated by linear interpolation of radiocarbon dates, 1963 and 1986 AD ^{137}Cs peaks and interpolated dates obtained for tie points in core 1A-1K

Table 1 Radiocarbon dates used for the construction of the age model for the Lake Estanya sequence

Comp depth (cm)	Laboratory code	Type of material	AMS ^{14}C age (years BP)	Calibrated age (cal years AD) (range 2σ)
28.5	Poz-24749	*Phragmites* stem fragment	155 ± 30	1790 ± 100
54.5	Poz-12245	Plant remains and charcoal	405 ± 30	1490 ± 60
170	Poz-12246	Plant remains	895 ± 35	1110 ± 60

Calibration was performed using CALPAL software and the INTCAL04 curve (Reimer et al. 2004); and the median of the 95.4% distribution (2σ probability interval) was selected

Table 2 Sedimentary facies and inferred depositional environment for the Lake Estanya sedimentary sequence

Facies	Sedimentological features	Depositional subenvironment
Clastic facies		
A	Alternating dark grey and black, massive, organic-rich silts, organized in cm-thick bands	Deep, freshwater to brackish and monomictic lake
B	Variegated, mm-thick laminated silts, alternating: (1) light grey, massive clays; (2) dark brown, massive organic-rich laminae; and (3) grey/brown massive silts	Deep, freshwater to brackish and dimictic lake
C	Dark grey, brownish, laminated silts with organic matter, organized in cm-thick bands	Deep, freshwater and monomictic lake
D	Grey, barely laminated silts with mm-thick intercalations of: (1) white, gypsum rich laminae; (2) brown, massive organic rich laminae; and occasionally (3) yellowish aragonite laminae	Deep, brackish to saline, dimictic lake
E	Black, massive to faintly laminated silty clay	Shallow lake with periodic flooding episodes and anoxic conditions
F	Dark-grey, massive silts with evidence of bioturbation and plant remains	Shallow, saline lake with periodic flooding episodes
Organic and gypsum-rich facies		
G	Brown, massive to faintly laminated sapropel with nodular gypsum	Shallow, saline lake with periodic flooding episodes
H	White to yellowish, massive gypsum laminae	

The sequence was divided into seven units according to sedimentary facies distribution (Figs. 2a; 4). The 161-cm-thick composite sequence, formed by cores 1A-1K and 1A-1M, is preceded by a 9-cm-thick, organic-rich deposit with nodular gypsum (unit 7, 170–161 cm composite depth). Unit 6 (160–128 cm, ~1140–1245 AD) is composed of alternating cm-thick bands of organic-rich facies G, gypsum-rich facies H and massive, clastic facies F, interpreted as deposition in a relatively shallow, saline lake with occasional runoff episodes, more frequent towards the top. The remarkable rise in linear sedimentation rate (LSR) in unit 6 from 0.3 mm/year during deposition of previous Unit II [defined in Morellón et al. (2009)] to 3.0 mm/year, reflects the dominance of detrital facies since medieval times (Fig. 3g). The next interval (Unit 5, 128–110 cm, ~1245–1305 AD) is characterized by the deposition of black, massive clays (facies E), reflecting fine-grained sediment input from the catchment, and dominant anoxic conditions at the lake bottom. The occurrence of a marked peak (31 SI units) in magnetic susceptibility (MS) might be related to an increase in iron sulphides formed under these conditions. This sedimentary unit is followed by a thicker interval (unit 4, 110–60 cm, ~1305–1470 AD) of laminated, relatively coarser clastic facies D,

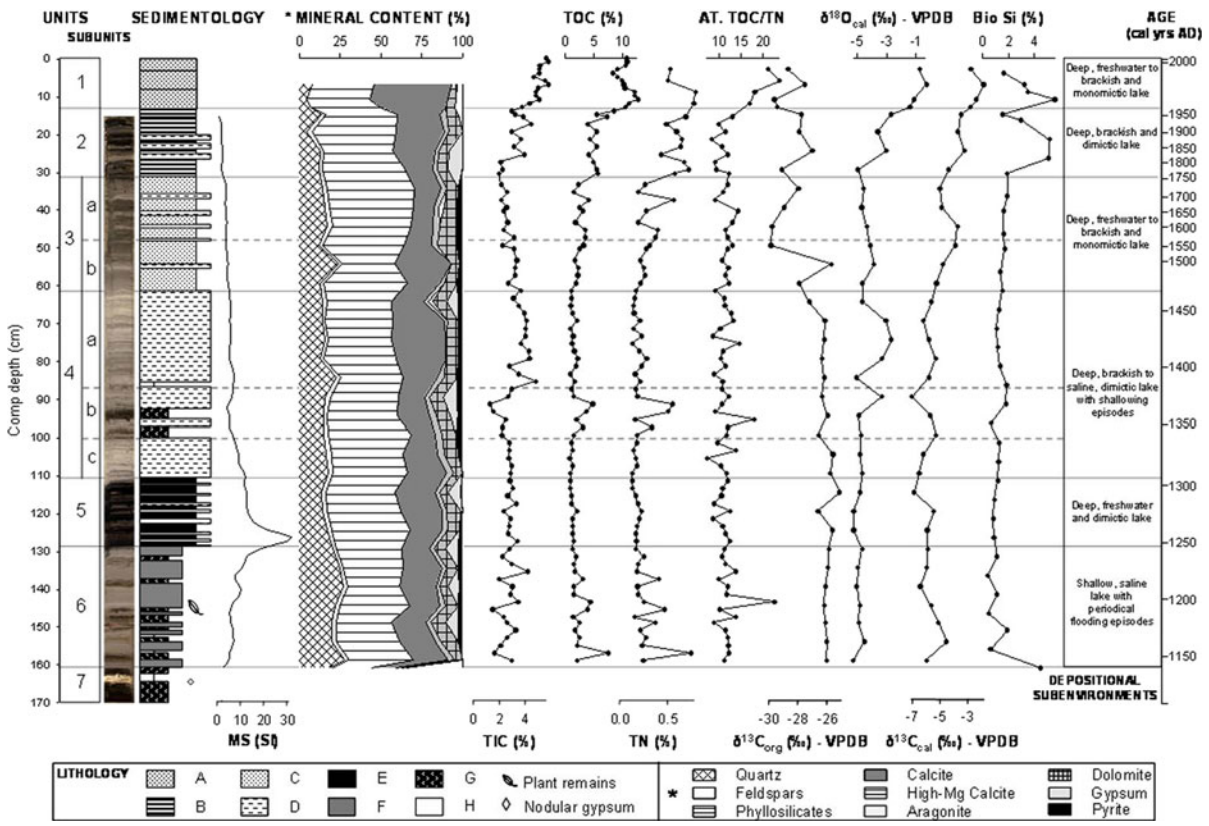

Fig. 4 Composite sequence of cores 1A-1M and 1A-1K for the studied Lake Estanya record. From left to right: Sedimentary units, available core images, sedimentological profile, Magnetic Susceptibility (MS) (SI units), bulk sediment mineralogical content (see legend below) (%); TIC, Total Inorganic Carbon (%); TOC, Total Organic Carbon (%); TN, Total Nitrogen (%); atomic TOC/TN ratio; bulk sediment $\delta^{13}C_{org}$, $\delta^{13}C_{calcite}$ and $\delta^{18}O_{calcite}$ (‰), referred to VPDB standard and biogenic silica concentration (BSi) and inferred depositional environments for each unit. Interpolated ages (cal yrs AD) are represented in the age scale at the right side

(subunits 4a and 4c) with some intercalations of gypsum and organic-rich facies G (subunit 4b), representing episodes of lower lake levels and more saline conditions. More dilute waters during deposition of subunit 4a are indicated by an upcore decrease in gypsum and high-magnesium calcite (HMC), and higher calcite content.

The following unit 3 (60–31 cm, ~1470–1760 AD) is characterized by the deposition of massive facies C, indicative of increased runoff and higher sediment delivery. The decrease in carbonate content (TIC, calcite), increase in organic matter and increase in clays and silicates is particularly marked in the upper part of the unit (3b) and correlates with a higher frequency of facies D, revealing increased siliciclastic input. The deposition of laminated facies B along unit 2 (31–13 cm, ~1760–1965 AD) and the parallel increase in carbonates and organic matter reflect increased organic and carbonate productivity (likely derived from littoral areas) during a period with predominantly anoxic conditions in the hypolimnion, limiting bioturbation. Reduced siliciclastic input is indicated by lower percentages of quartz, clays and oxides. Average LSR during deposition of units 3 and 2 is the lowest (~0.8 mm/year). Finally, deposition of massive facies A, with the highest carbonate, organic matter and LSR (3.41 mm/year) values during the uppermost unit 1 (13–0 cm, after ~1965 AD) suggests less frequent anoxic conditions in the lake bottom, and large input of littoral and watershed-derived organic and carbonate material, similar to the present-day conditions (Morellón et al. 2009).

Organic geochemistry

TOC, TN and atomic TOC/TN ratio

The organic content of Lake Estanya sediments is highly variable, ranging from 1 to 12% TOC (Fig. 4). Lower values (up to 5%) occur in lowermost units 6, 5 and 4. The intercalation of two layers of facies F within clastic-dominated unit 4 results in two peaks of 3–5%. A rising trend started at the base of unit 3 (from 3 to 5%), characterized by the deposition of facies C, continued with relatively high values in unit 2 (facies B) and reached the highest values in the uppermost 13 cm (unit 1, facies A) (Fig. 4). TOC/TN values around 13 indicate that algal organic matter dominates over terrestrial plant remains derived from the catchment (Meyers and Lallier-Vergès 1999). Lower TOC/TN values occur in some levels where an even higher contribution of the algal fraction is suspected, as in unit 2. The higher values in unit 1 indicate a large increase in the input of carbon-rich, terrestrial organic matter.

Stable isotopes in organic matter

The range of $\delta^{13}C_{org}$ values (−25 to −30‰) also indicates that organic matter is mostly of lacustrine origin (Meyers and Lallier-Vergès 1999), although influenced by land-derived vascular plants in some intervals. Isotope values remain constant, centred around −25‰ in units 6–4, and experience an abrupt decrease at the base of unit 3, leading to values around −30‰ at the top of the sequence (Fig. 4). Parallel increases in TOC/TN and decreasing $\delta^{13}C_{org}$ confirm a higher influence of vascular plants from the lake catchment in the organic fraction during deposition of the uppermost three units. Thus, $\delta^{13}C_{org}$ fluctuations can be interpreted as changes in organic matter sources and vegetation type, rather than as changes in trophic state and productivity of the lake. Negative excursions of $\delta^{13}C_{org}$ represent increased land-derived organic matter input. However, the relative increase in $\delta^{13}C_{org}$ in unit 2, coinciding with the deposition of laminated facies B, could be a reflection of both reduced influence of transported terrestrial plant detritus (Meyers and Lallier-Vergès 1999), but also an increase in biological productivity in the lake, as indicated by other proxies.

Biogenic silica (BSi)

The opal content of the Lake Estanya sediment sequence is relatively low, oscillating between 0.5 and 6%. BSi values remain stable around 1% along units 6 to 3, and sharply increase, reaching 5% in units 2 and 1. However, relatively lower values occur at the top of both units (Fig. 4). Fluctuations in BSi content mainly record changes in primary productivity of diatoms in the euphotic zone (Colman et al. 1995; Johnson et al. 2001). Coherent relative increases in TN and BSi, together with relatively higher $\delta^{13}C_{org}$ indicate enhanced algal productivity in these intervals.

Inorganic geochemistry

XRF core scanning of light elements

The downcore profiles of light elements (Al, Si, P, S, K, Ca, Ti, Mn and Fe) in core 5A-1U correspond with sedimentary facies distribution (Fig. 5a). Given their low values and "noisy" behaviour, P and Mn were not included in the statistical analyses. According to their relationship with sedimentary facies, three main groups of elements can be observed: (1) Si, Al, K, Ti and Fe, with variable, but predominantly higher values in clastic-dominated intervals; (2) S, associated with the presence of gypsum-rich facies; and (3) Ca, which displays maximum values in gypsum-rich facies and carbonate-rich sediments. The first group shows generally high but fluctuating values along basal unit 6, as a result of the intercalation of gypsum-rich facies G and H and clastic facies F, and generally lower and constant values along units 5–3, with minor fluctuations as a result of intercalations of facies G (around 93 and 97 cm in core 1A-1K, and at 130–140 cm in core 5A-1U core depth). After a marked positive excursion in subunit 3a, the onset of unit 2 marks a clear decreasing trend up to unit 1. Calcium (Ca) shows the opposite behaviour, peaking in unit 1, the upper half of unit 2, some intervals of subunit 3b and 4, and in the gypsum–rich unit 6. Sulphur (S) displays low values, near 0, throughout the sequence, peaking when gypsum-rich facies G and H occur, mainly in units 6 and 4.

Principal component analyses (PCA)

Principal Component Analysis (PCA) was carried out using this elemental dataset (7 variables and 216

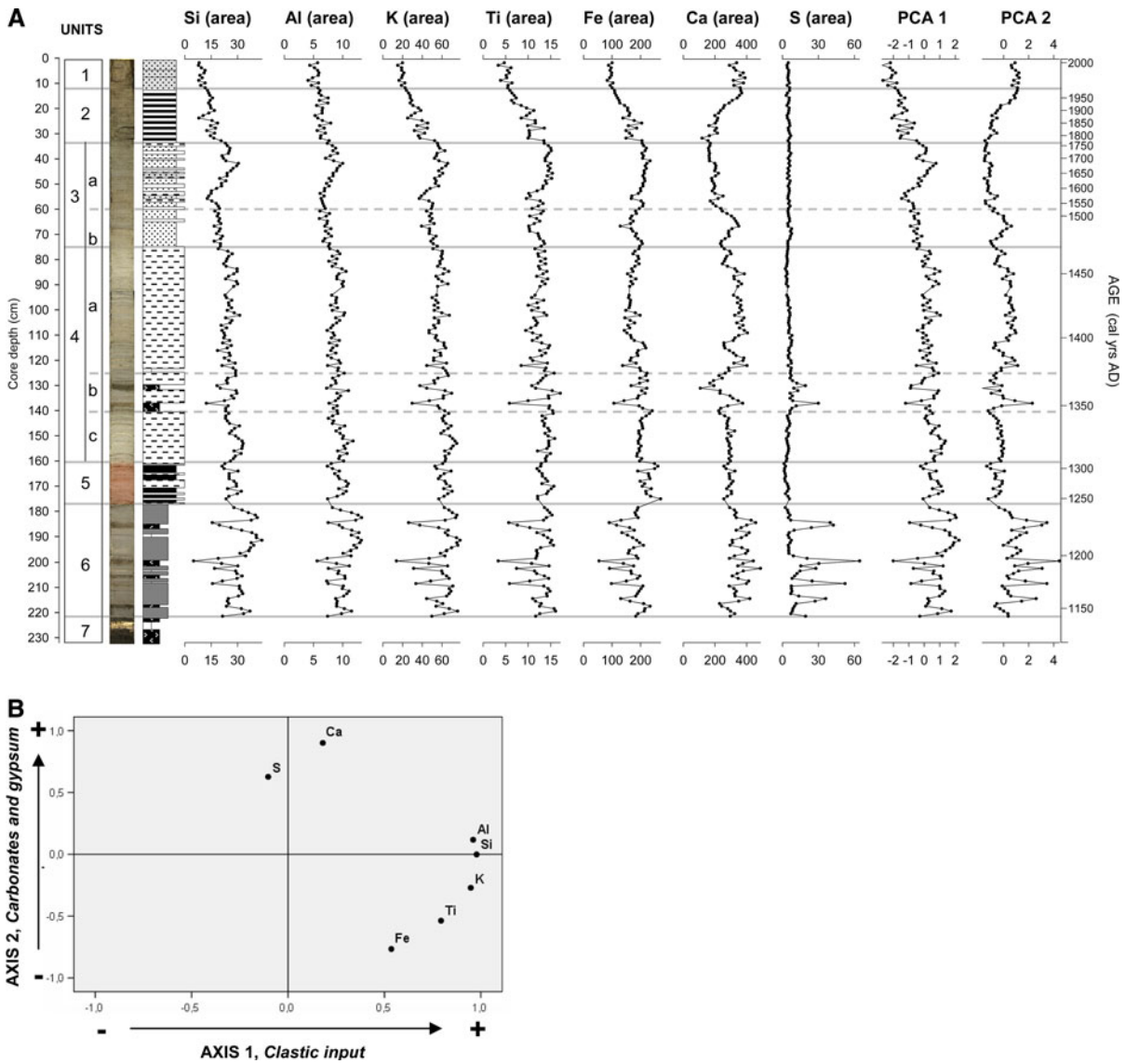

Fig. 5 **a** X-ray fluorescence (XRF) data measured in core 5A-1U by the core scanner. Light elements (Si, Al, K, Ti, Fe, S and Ca) concentrations are expressed as element intensities (areas) $\times 10^2$. Variations of the two-first eigenvectors (PCA1 and PCA2) scores against core depth have also been plotted as a synthesis of the XRF variables. Sedimentary units and subunits, core image and sedimentological profile are also indicated (see legend in Fig. 4). Interpolated ages (cal yrs AD) are represented in the age scale at the right side. **b** Principal Components Analysis (PCA) projection of factor loads for the X-Ray Fluorescence analyzed elements. *Dots* represent the factor loads for every variable in the plane defined by the first two eigenvectors

cases). The first two eigenvectors account for 84.3% of the total variance (Table 3a). The first eigenvector represents 59.1% of the total variance, and is controlled mainly by Al, Si and K, and secondarily by Ti and Fe at the positive end (Table 3; Fig. 5b). The second eigenvector accounts for 25.3% of the total variance and is mainly controlled by S and Ca, both at the positive end (Table 3; Fig. 5b). The other eigenvectors defined by the PCA analysis were not included in the interpretation of geochemical variability, given that they represented low percentages of the total variance (<20%; Table 3a). As expected, the PCA analyses clearly show that: (1) Al, Si, Ti and Fe have a common origin, likely related to their

Table 3 Principal Component Analysis (PCA) (a) Eigenvalues for the seven obtained components. The percentage of the variance explained by each axis is also indicated; (b) Factor loads for every variable in the two main axes

Component	Initial eigenvalues		
	Total	% of variance	% Cumulative
(**a**)			
1	4.135	59.072	59.072
2	1.768	25.256	84.329
3	0.741	10.582	94.911
	Component		
	1	2	
(**b**)			
Si	0.978	−0.002	
Al	0.960	0.118	
K	0.948	−0.271	
Ti	0.794	−0.537	
Ca	0.180	0.900	
Fe	0.536	−0.766	
S	−0.103	0.626	

presence in silicates, represented by eigenvector 1 and (2) Ca and S display a similar pattern as a result of their occurrence in carbonates and gypsum, represented by eigenvector 2.

The location of every sample with respect to the vectorial space defined by the two-first PCA axes and their plot with respect to their composite depth (Giralt et al. 2008; Muller et al. 2008) allow us to reconstruct, at least qualitatively, the evolution of clastic input and carbonate and gypsum deposition along the sequence (Fig. 5a). Positive scores of eigenvector 1 represent increased clastic input, and display maximum values when clastic facies A, B, C, D and E occur, along units 6–3, and a decreasing trend from the middle part of unit 3 until the top of the sequence (Fig. 5a). Positive scores of eigenvector 2 indicate higher carbonate and gypsum content and display highest values when gypsum-rich facies G and H occur as intercalations in units 6 and 4, and in the two uppermost units (1 and 2) coinciding with increased carbonate content in the sediments (Figs. 4, 5a). The depositional interpretation of this eigenvector is more complex because both endogenic and reworked littoral carbonates contribute to carbonate sedimentation in distal areas.

Stable isotopes in carbonates

Interpreting calcite isotope data from bulk sediment samples is often complex because of the different sources of calcium carbonate in lacustrine sediments (Talbot 1990). Microscopic observation of smear slides documents three types of carbonate particles in the Lake Estanya sediments: (1) biological, including macrophyte coatings, ostracod and gastropod shells, *Chara* spp. remains and other bioclasts, reworked from carbonate-producing littoral areas of the lake (Morellón et al. 2009), (2) small (10 μm), locally abundant, rice-shaped endogenic calcite grains; and (3) allochthonous calcite and dolomite crystals derived from carbonate bedrock, sediments and soils in the watershed.

The isotopic composition of the Triassic limestone bedrock is characterized by relatively low oxygen isotope values (between −4.0 and −6.0‰; average $\delta^{18}O_{calcite} = -5.3‰$), and negative, but variable carbon values ($-6.9‰ < \delta^{13}C_{calcite} < -0.7‰$), whereas modern endogenic calcite in macrophyte coatings displays significantly heavier oxygen and carbon values ($\delta^{18}O_{calcite} = +2.3‰$ and $\delta^{13}C_{calcite} = -1.3‰$; Fig. 6a). The isotopic composition of this calcite is approximately in equilibrium with lake waters, which are significantly enriched in ^{18}O (averaging 1.0‰), compared to Estanya spring (−8.0‰), and Estanque Grande de Arriba (−3.4‰), thus indicating a long residence time, characteristic of endorheic, brackish to saline lakes (Fig. 6b). Although values of $\delta^{13}C_{DIC}$ experience higher variability, as a result of changes in organic productivity throughout the water column, as occurs in other seasonally stratified lakes (Leng and Marshall 2004) (Fig. 6c), the $\delta^{13}C$ composition of modern endogenic calcite in Lake Estanya (−1.3‰) is also consistent with precipitation from surface waters with dissolved inorganic carbon (DIC) relatively enriched in heavier isotopes.

Bulk sediment samples from units 6, 5 and 3 show $\delta^{18}O_{calcite}$ values (−7.1‰ to −3.2‰) similar to the isotopic signal of the bedrock (−4.6‰ to −5.2‰), indicating a dominant clastic origin of the carbonate. Parallel evolution of siliciclastic mineral content (quartz, feldspars and phylosilicates) and calcite also points to a dominant allochthonous origin of calcite in these intervals. Only subunits 4a and b and uppermost units 1 and 2 lie out of the bedrock range and are closer to endogenic calcite, reaching

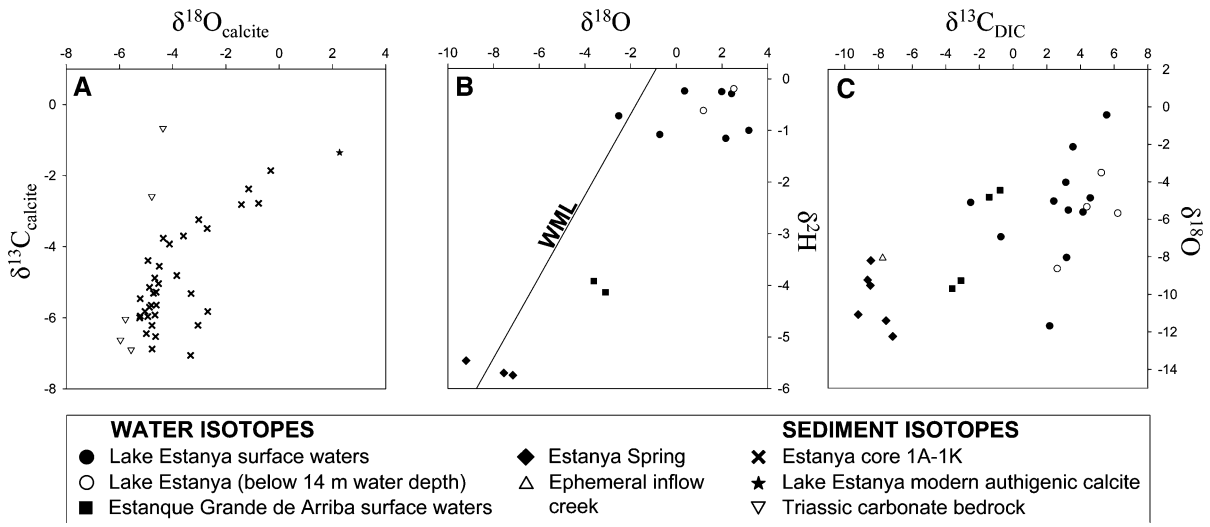

Fig. 6 Isotope survey of Lake Estanya sediment, bedrock and waters. **a** $\delta^{13}C_{calcite}$–$\delta^{18}O_{calcite}$ cross plot of composite sequence 1A-1M/1A-1K bulk sediment samples, carbonate bedrock samples and modern endogenic calcite macrophyte coatings (see legend). **b** $\delta^{2}H$–$\delta^{18}O$ cross-plot of rain, Estanya Spring, small Estanque Grande de Arriba Lake and Lake Estanya surface and bottom waters. **c** $\delta^{13}C_{DIC}$–$\delta^{18}O$ cross-plot of these water samples. All the isotopic values are expressed in ‰ and referred to the VPDB (carbonates and organic matter) and SMOW (water) standards

maximum values of −0.3‰ (Figs. 4, 6a). In the absence of contamination sources, the two primary factors controlling $\delta^{18}O_{calcite}$ values are moisture balance (precipitation minus evaporation) and the isotopic composition of lake waters (Griffiths et al. 2002), although pH and temperature can also be responsible for some variations (Zeebe 1999). The positive $\delta^{18}O_{calcite}$ excursions during units 4, 2 and 1 correlate with increasing calcite content and the presence of other endogenic carbonate phases (HMC; Fig. 4), and suggest that during those periods the contribution of endogenic calcite, either from the littoral zone or the epilimnion, to the bulk sediment isotopic signal was higher.

The $\delta^{13}C_{calcite}$ curve also reflects detrital calcite contamination through lowermost units 6 and 5, characterized by relatively low values (−4.5‰ to −7.0‰). However, the positive trend from subunit 4a to the top of the sequence (−6.0‰ to −1.9‰) correlates with enhanced biological productivity, as reflected by TOC, TN, BSi and $\delta^{13}C_{org}$ (Fig. 4). Increased biological productivity would have led to higher DIC values in water and then, precipitation of isotopically ^{13}C-enriched calcite (Leng and Marshall 2004).

Diatom stratigraphy

Diatom preservation was relatively low, with sterile samples at some intervals, and from 25 to 90% of specimens affected by fragmentation and/or dissolution. Nevertheless, valve concentrations (VC), the centric vs. pennate (C:P) diatom ratio, relative concentration of *Campylodiscus clypeus* fragments (CF), and changes in dominant taxa, allowed us to distinguish the most relevant features in the diatom stratigraphy (Fig. 7). BSi concentrations (Fig. 4) are consistent with diatom productivity estimates. However, larger diatoms contain more BSi than smaller ones and thus, absolute VCs and BSi are comparable only within communities of similar taxonomic composition (Figs. 4, 7). The C:P ratio was used mainly to determine changes among predominantly benthic (littoral or epiphytic) and planktonic (floating) communities, although we are aware that it may also reflect variation in the trophic state of the lacustrine ecosystem (Cooper 1995). Together with BSi content, strong variations of this index indicated periods of large fluctuations in lake level, water salinity and lake trophic status. The relative content of CF represents the extension of brackish-saline and benthic environments

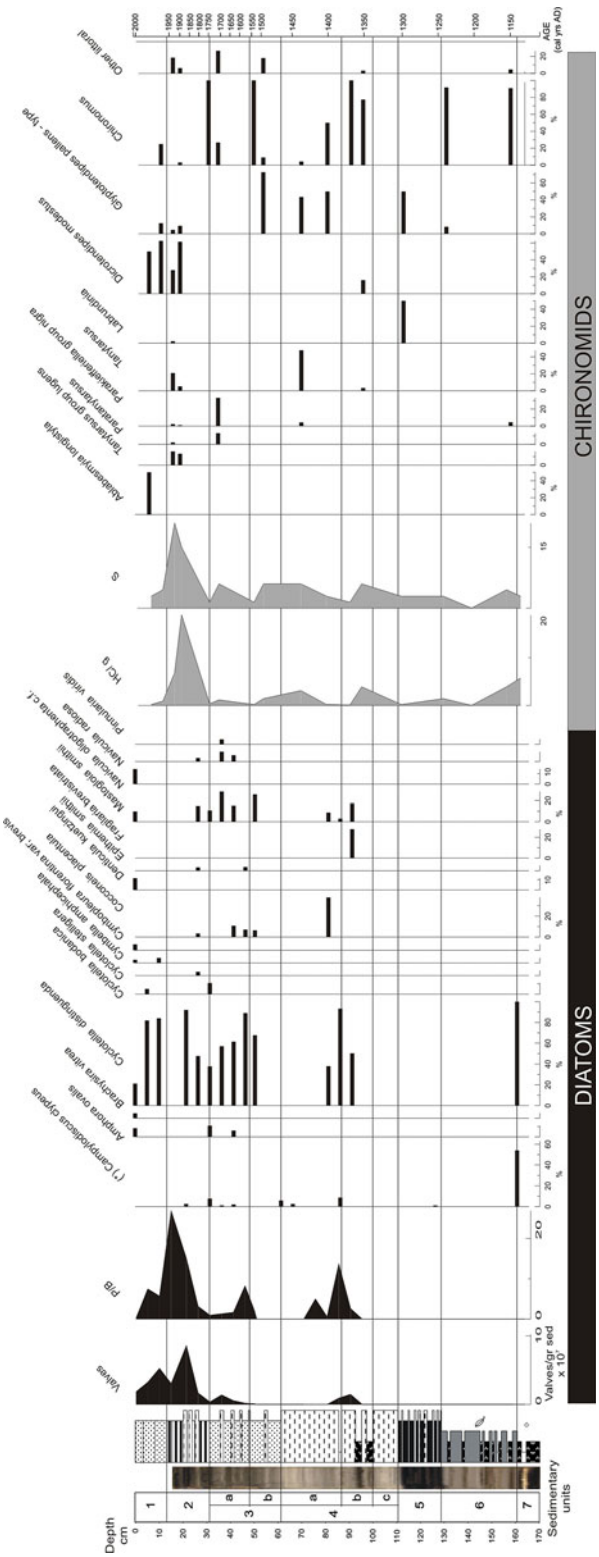

Fig. 7 Selected taxa of diatoms (*black*) and chironomids (*grey*) stratigraphy for the composite sequence 1A-1M/1A-1K. Sedimentary units and subunits, core image and sedimentological profile are also indicated (see legend in Fig. 4). (*) *Campylodiscus clypeus* abundance is reflected as a percentage of examined microscope fields of view with valve fragments

(Risberg et al. 2005; Saros et al. 2000; Witak and Jankowska 2005).

Description of the main trends in the diatom stratigraphy of the Lake Estanya sequence (Fig. 7) was organized following the six sedimentary units previously described. Diatom content in lower units 6, 5 and 4c is very low. The onset of unit 6 is characterized by a decline in VC and a significant change from the previously dominant saline and shallow environments, indicated by high CF (>50%), low valve content, and presence of *Cyclotella distinguenda* and *Navicula* sp. The decline in VC suggests adverse conditions for diatom development (hypersaline, ephemeral conditions, high turbidity due to increased sediment delivery, and/or preservation related to high alkalinity). Adverse conditions continued during deposition of units 5 and subunit 4c, where diatoms are absent or present only in trace numbers.

The reappearance of CF and the increase in VC and productivity (BSi) mark the onset of a significant limnological change in the lake during deposition of unit 4b. Although the dominance of CF suggests early development of saline conditions, soon the diatom assemblage changed and the main taxa were *C. distinguenda*, *Fragilaria brevistriata* and *Mastogloia smithii* at the top of subunit 4b, reflecting less saline conditions and more alkaline pH values. The C:P > 1 suggests the prevalence of planktonic diatoms associated with relatively higher water levels. In the lower part of subunit 4a, VC and diatom productivity dropped. *C. distinguenda* is replaced by *Cocconeis placentula*, an epiphytic and epipelic species, and then by *M. smithii*. This succession indicates the proximity of littoral hydrophytes and thus, shallower conditions. Diatoms are absent or only present in small numbers at the top of subunit 4a, marking the return of adverse conditions for survival or preservation, that persisted during deposition of subunit 3b. The onset of subunit 3a corresponds to a marked increase in VC; the relatively high percentages of *C. distinguenda*, *C. placentula* and *M. smithii* suggest the increasing importance of pelagic environments, and thus, higher lake levels. Other species appear in unit 3a, the most relevant being *Navicula radiosa*, which seems to prefer oligotrophic water, and *Amphora ovalis* and *Pinnularia viridis*, commonly associated with lower-salinity environments. After a small peak around 36 cm, VC diminishes towards the top of the unit. The reappearance of CF during a short period at the transition between units 3 and 2 indicates increased salinity.

Unit 2 starts with a marked increase in VC, reaching the highest value throughout the sequence and coinciding with a large BSi peak. *C. distinguenda* became the dominant species, epiphytic diatoms decline, and CF disappears. This change suggests the development of a larger, deeper lake. The pronounced decline in VC towards the top of the unit and the appearance of *Cymbella amphipleura*, an epiphytic species, is interpreted as a reduction of pelagic environments in the lake.

Top unit 1 is characterized by a strong decline in VC. The simultaneous occurrence of a BSi peak and decline of VC may be associated with an increase in diatom size, as indicated by lowered C:P (<1). Although *C. distinguenda* remains dominant, epiphytic species are also abundant. Diversity increases, with the presence of *Cymbopleura florentina* nov. comb. nov. stat., *Denticula kuetzingui*, *Navicula oligotraphenta*, *A. ovalis, Brachysira vitrea* and the reappearance of *M. smithii,* all found in the present-day littoral vegetation (unpublished data). Therefore, top diatom assemblages suggest development of extensive littoral environments in the lake, and thus relatively shallower conditions compared to unit 2.

Chironomid stratigraphy

Overall, 23 chironomid species were found in the sediment sequence. The more frequent and abundant taxa were *Dicrotendipes modestus*, *Glyptotendipes pallens*-type, *Chironomus*, *Tanytarsus*, *Tanytarsus* group *lugens* and *Parakiefferiella* group *nigra.* In total, 289 chironomid head capsules (HC) were identified. Densities were generally low (0–19 HC/g), and abundances per sample varied between 0 and 96 HC. The species richness (*S*, number of species per sample) ranged between 0 and 14. Biological zones defined by the chironomid assemblages are consistent with sedimentary units (Fig. 7).

Low abundances and species numbers (*S*), and predominance of *Chironomus*, characterize Unit 6. This midge is one of the most tolerant to low dissolved oxygen conditions (Brodersen et al. 2008). In temperate lakes, this genus is associated with soft surfaces and organic-rich sediments in deep water (Saether 1979), or with unstable sediments in

shallower lakes (Brodersen et al. 2001). However, in deep karstic Iberian lakes, anoxic conditions are not directly related with trophic state, but with oxygen depletion due to longer stratification periods (Prat and Rieradevall 1995), when *Chironomus* can become dominant. In brackish systems, osmoregulatory stress exerts a strong effect on macrobenthic fauna, which is expressed in very low diversities (Verschuren et al. 2000). Consequently, the development of *Chironomus* in Lake Estanya during unit 6 is more likely related to the abundance of shallower, disturbed bottom with higher salinity.

The total absence of deep-environment representatives, the very low densities and S during deposition of Unit 5 (~1245–1305 AD) might indicate extended, permanent anoxic conditions that impeded establishment of abundant and diverse chironomid assemblages and only very shallow areas available for colonization by *Labrundinia* and *G. pallens*-type. In Unit 4, chironomid remains present variable densities, with *Chironomus,* accompanied by the littoral *D. modestus* in subunit 4b, and *G. pallens*-type and *Tanytarsus* in subunit 4a. Although *Glyptotendipes* has been generally associated with the presence of littoral macrophytes and charophytes, it has been suggested that this taxon can also reflect conditions of shallow, highly productive and turbid lakes, with no aquatic plants, but organic sediments (Brodersen et al. 2001).

A significant change in chironomid assemblages occurs in unit 3, characterized by the increased presence of littoral taxa absent in previous intervals. *Chironomus* and *G. pallens*-type are accompanied by *Paratanytarsus, Parakiefferiella* group *nigra*, and other epiphytic or shallow-environment species (e.g. *Psectrocladius sordidellus*, *Cricotopus obnixus*, *Polypedilum* group *nubifer*). Considering the Lake Estanya bathymetry and the funnel-shaped basin morphology (Figs. 2a, 3c), a large increase in shallow areas available for littoral species colonization could only occur with a considerable lake level increase and the flooding of the littoral platform. An increase in shallower, littoral environments with disturbed sediments is likely to have occurred at the transition to unit 2 where *Chironomus* is the only species present in the record.

The largest change in chironomid assemblages occurred in Unit 2, which has the highest HC concentration and S throughout the sequence, indicative of high biological productivity. The low relative abundance of species representative of deep environments could indicate the development of large littoral areas and prevalence of anoxic conditions in the deepest areas. Some species, such as *Chironomus*, would be greatly reduced. The chironomid assemblages in the uppermost part of unit 2 reflect heterogeneous littoral environments, with up to 17 species characteristic of shallow waters, and *D. modestus* as the dominant species. In Unit 1, chironomid abundance decreases again. The presence of the tanypodini *A. longistyla* and the littoral chironomini *D. modestus*, reflects a shallowing trend, initiated at the top of unit 2.

Pollen stratigraphy

The pollen of the Estanya sequence is characterized by marked changes in three main vegetation groups (Fig. 8): (1) conifers (mainly *Pinus* and *Juniperus*) and mesic and Mediterranean woody taxa, (2) cultivated plants and ruderal herbs, and (3) aquatic plants. Conifers, woody taxa and shrubs, including both mesic and Mediterranean components, reflect the regional landscape composition. Among the cultivated taxa, olive trees, cereals, grapevines, walnut and hemp are dominant, accompanied by ruderal herbs (*Artemisia*, Asteroideae, Cichorioideae, Carduae, *Centaurea, Plantago, Rumex*, Urticaceae, etc.), indicating both farming and pastoral activities. Finally, hygrophytes and riparian plants (*Tamarix, Salix, Populus*, Cyperaceae and *Typha*) and hydrophytes (*Ranunculus, Potamogeton, Myriophyllum, Lemna* and *Nuphar*) reflect changes in the limnic and littoral environments and are represented as HH in the pollen diagram (Fig 8). Some components included in the Poaceae curve could also be associated with hygrophytic vegetation (*Phragmites*). Due to the particular funnel-shape morphology of Lake Estanya, increasing percentages of riparian and hygrophytic plants may occur during periods of both higher and lower lake level. However, the different responses of these vegetation types allows one to distinguish between the two lake stages: (1) during low water levels, riparian and hygrophyte plants increase, but the relatively small development of littoral areas causes a decrease in hydrophytes; and (2) during high-water-level phases, involving the flooding of the large littoral platform, increases in the

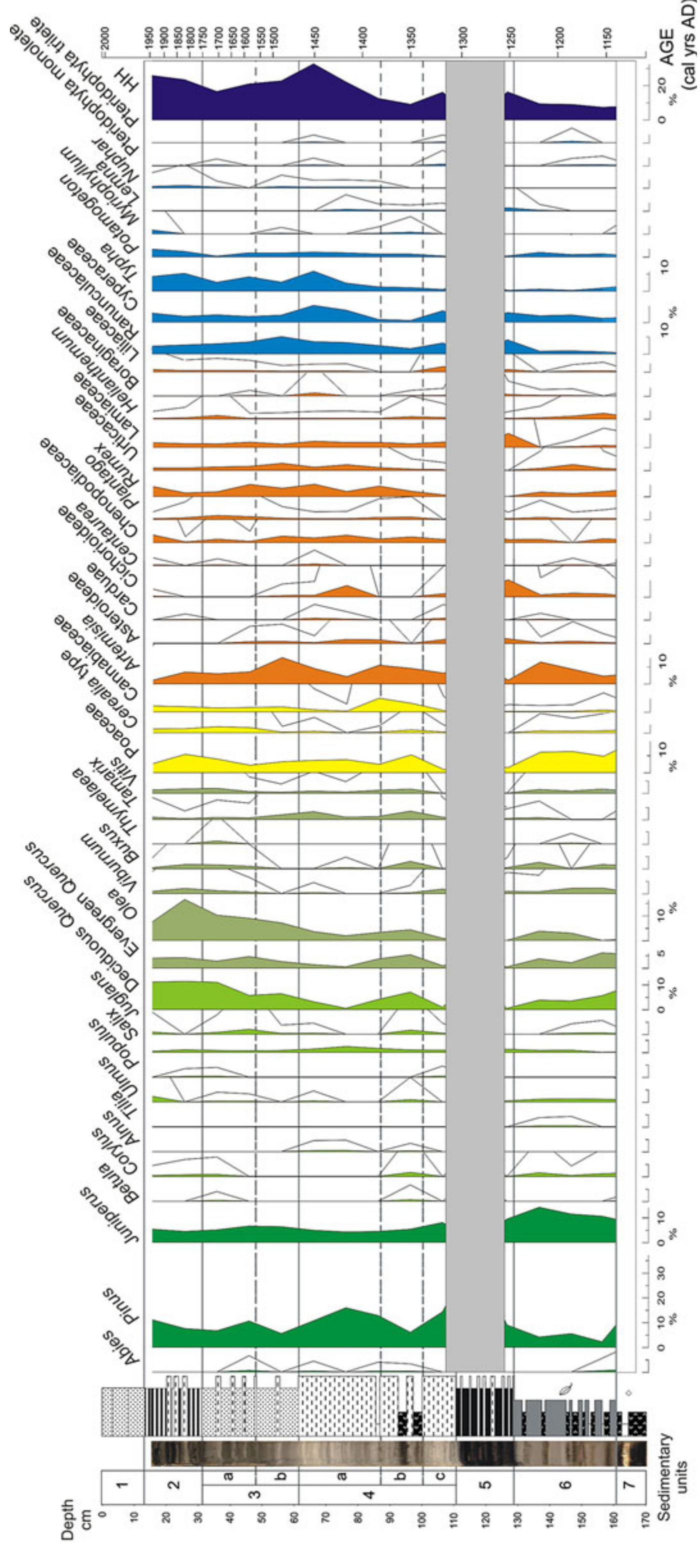

Fig. 8 Selected pollen taxa diagram for the composite sequence 1A-1M/1A-1K, comprising units 2–6. Sedimentary units and subunits, core image and sedimentological profile are also indicated (see legend in Fig. 4). A grey horizontal band over unit 5 marks a low pollen content and high charcoal concentration

first group are also accompanied by high abundance and diversity of hydrophytes.

The main zones in the pollen stratigraphy are consistent with the sedimentary units (Fig. 8). Pollen in unit 6 shows a clear *Juniperus* dominance among conifers and arboreal pollen (AP). Deciduous *Quercus* and other mesic woody taxa are present in low proportions, including the only presence of *Tilia* along the sequence. Evergreen *Quercus* and Mediterranean shrubs as *Viburnum, Buxus* and *Thymelaea* are also present, and the heliophyte *Helianthemum* shows its highest percentages in the record. These pollen spectra suggest warmer and drier conditions than present. The aquatic component is poorly developed, pointing to lower lake levels than today. Cultivated plants are varied, but their relative percentages are low, as for plants associated with grazing activity (ruderals). *Cerealia* and *Vitis* are present throughout the sequence, consistent with the well-known expansion of vineyards throughout southern Europe during the High Middle Ages (eleventh to thirteenth century) (Guilaine 1991; Ruas 1990). There are no references to olive cultivation in the region until the mid eleventh century, and the main development phase occurred during the late twelfth century (Riera et al. 2004), coinciding with the first *Olea* peak in the Lake Estanya sequence, thus supporting our age model. The presence of *Juglans* is consistent with historical data reporting walnut cultivation and vineyard expansion contemporaneous with the founding of the first monasteries in the region before the ninth century (Esteban-Amat 2003).

Unit 5 has low pollen quantity and diversity, abundant fragmented grains, and high microcharcoal content (Fig. 8). All these features point to the possible occurrence of frequent forest fires in the catchment. Riera et al. (2004, 2006) also documented a charcoal peak during the late thirteenth century in a littoral core. In this context, the dominance of *Pinus* reflects differential pollen preservation caused by fires and thus, taphonomic over-representation (*grey band* in Fig. 8). Regional and littoral vegetation along subunit 4c is similar to that recorded in unit 6, supporting our interpretation of unit 5 and the relationship with forest fires. In subunit 4c, conifers dominate the AP group, but mesic and Mediterranean woody taxa are present in low percentages. Hygrohydrophytes increase and cultivated plant percentages are moderate, with a small increase in *Olea, Juglans, Vitis, Cerealia* and Cannabiaceae (Fig. 8).

More humid conditions in subunit 4b are interpreted from the decrease of conifers (junipers and pines, presence of *Abies*) and the increase in abundance and variety of mesophilic taxa (deciduous *Quercus* dominates, but the presence of *Betula, Corylus, Alnus, Ulmus* or *Salix* is important). Among the Mediterranean component, evergreen *Quercus* is still the main taxon; *Viburnum* decreases and *Thymelaea* disappears. The riparian formation is relatively varied and well developed, composed by *Salix, Tamarix*, some Poaceae, and Cyperaceae and *Typha* in minor proportions. All these features, together with the presence of *Myriophyllum, Potamogeton, Lemna* and *Nuphar* indicate increasing, but fluctuating lake levels. Cultivated plants (mainly cereals, grapevines and olive trees, but also *Juglans* and *Cannabis*) increase (Fig. 8). According to historical documents, hemp cultivation in the region started about the twelfth century (base of the sequence) and expanded ca. 1342 (Jordán de Asso y del Río 1798), which correlates with the *Cannabis* peak at 95 cm depth (Fig. 8).

Subunit 4a is characterized by a significant increase of *Pinus* (mainly the cold *nigra-sylvestris* type) and a decrease in mesophilic and thermophilic taxa, both types of *Quercus* reach their minimum values and only *Alnus* remains present as a representative of the deciduous formation. A decrease of *Juglans, Olea, Vitis, Cerealia* type and *Cannabis*, reflects a decline in agricultural production due to adverse climate and/or low population pressure in the region (Lacarra 1972; Riera et al. 2004). The clear increase of the riparian and hygrophyte component (*Salix, Tamarix*, Cyperaceae and *Typha* peak) imply the highest percentages of littoral vegetation along the sequence (Fig. 8), indicating shallower conditions.

More temperate conditions and an increase in human activities in the region can be inferred for the upper three units of the Lake Estanya sequence. An increase in anthropogenic activities occurred at the base of subunit 3b ($\sim$1470 AD) with an expansion of *Olea*, [synchronous with an *Olea* peak reported by Riera et al. (2004)], relatively high *Juglans, Vitis, Cerealia* type and *Cannabis* values, and an important ruderal component associated with pastoral and agriculture activities (*Artemisia,* Asteroideae, Cichorioideae, *Plantago, Rumex,* Chenopodiaceae, Urticaceae, etc.). In addition, more humid conditions are suggested by the increase in deciduous *Quercus* and aquatic

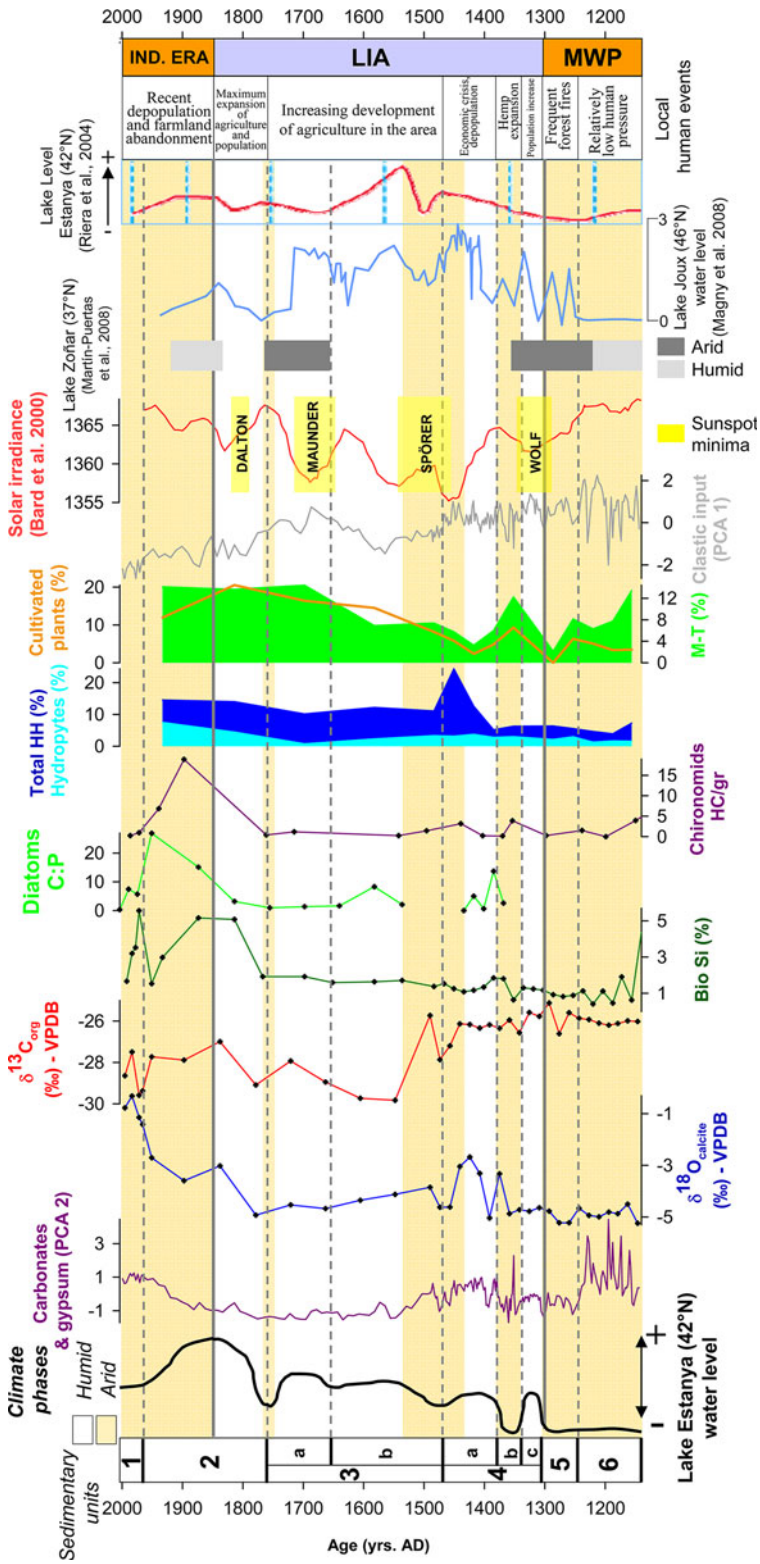

Fig. 9 Comparison of selected proxies of Lake Estanya sequence with other global and local paleorecords (last 800 years). From bottom to top: **a** sedimentary units (1–6) and subunits defined for the sediment sequence, synthetic curve of lake level evolution interpreted from the whole suite of proxies used in this research, geochemically-based carbonates and gypsum content (PCA axis 2 derived from XRF data), $\delta^{18}O_{calcite}$ (‰), $\delta^{13}C_{org}$ (‰), BSi (%), diatoms C:P ratio, hydrophytes concentration with respect to total aquatic plants (hygro-hydrophytes, HH) pollen concentration (%), mesophylic pollen and cultivated pollen taxa (%) and geochemically-based clastic input reconstruction (PCA axis 2 derived from XRF data). **b** From bottom to top: total solar irradiance (Bard et al. 2000) and main phases of solar minima (*yellow horizontal bars*), arid and humid phases interpreted from the Lake Zoñar record (Martín-Puertas et al. 2008), water level reconstruction for Lake Joux (Magny et al. 2008) and Estanya lake level reconstruction based on an aquatic pollen model (Riera et al. 2004). Vertical solid lines represent limits between the three main environmental stages in the evolution of the lake, whereas vertical shaded bars represent the main arid phases interpreted from the Lake Estanya record (see legend). Temporal divisions Medieval Warm Period (MWP), Little Ice Age (LIA) and Industrial Era (IND. ERA) are also indicated at the uppermost part of the figure

plants (Ranunculaceae, *Potamogeton, Myriophyllum, Nuphar*), in conjunction with the decrease of the hygrophyte component (Fig. 9). The expansion of aquatic taxa was likely caused by flooding of the littoral shelf during higher water levels. Finally, a warming trend is inferred from the decrease in conifers (previously dominated by *Pinus nigra-sylvestris* type in unit 4), and the development of evergreen *Quercus.*

During subunit 3a, cultivars, AP and the Mediterranean component increase (Fig. 8), both in terms of relative percentages and composition (*Betula, Corylus, Ulmus, Populus, Salix*, and deciduous *Quercus* as mesophylic woody taxa, and *Viburnum, Buxus, Thymelaea* or *Helianthemum* among the thermophylic components). A brief episode of Hydrohygrophytes (HH) decrease at the transition to unit 2 (Figs. 8, 9) may correspond to a small lake level fluctuation. Higher proportions of *Olea, Vitis* and *Cerealia* type indicate more intense cultivation in the watershed; a coincident decrease in some ruderal herbs suggests a change in farming and grazing activities.

The uppermost part of the palynological sequence (lower half of unit 2) represents the maximum expansion of cultivated areas during the nineteenth century, followed by a decrease in agricultural activity (top half of unit 2) during the late nineteenth century. The pollen of hydrological indicators (HH group) reflect an increase in water depth and an expansion of littoral environments as riparian (*Populus, Salix, Tamarix*), hygrophytes (Cyperaceae, *Typha* and some Poaceae) and hydrophytes (Ranunculaceae, *Potamogeton, Myriophyllum, Nuphar*) are well represented. Regional vegetation is a mixed Mediterranean formation in an open, patchy landscape similar to the present, with conifers (pines and junipers), deciduous, and mesophylic trees developed in humid or shady areas and evergreen oaks in sunny exposures.

Discussion

Our multiproxy study of the 800-year Lake Estanya sequence used a robust chronology to develop a higher-resolution reconstruction than was possible in previous regional (Davis 1994) and local studies (Riera et al. 2004, 2006). Our approach included sedimentological, geochemical and biological proxies. The chronology of the main climate episodes during the last millennium, particularly the MWP and the LIA, particularly in the western Mediterranean, are not well constrained, although available data suggest a high regional variability on the Iberian Peninsula (IP) (Álvarez et al. 2005; Desprat et al. 2003). Anthropogenic impacts on the landscape, vegetation cover, and hydrology also have a strong regional variability component and, very likely, lake responses to climate change were modulated by human activities.

Inferred paleoclimate, paleoenvironment and paleohydrologic changes in Lake Estanya are in general agreement with regional patterns (Luterbacher et al. 2005): more arid climate up to the fourteenth century; a rapid transition to more humid and colder climates during a period with high variability that lasted up to the mid-late nineteenth century, and a rapid transition to a warmer and less humid climate during the last century. The varying intensity of human impact on the landscape and Lake Estanya hydrology was influenced by economic and social factors as well as climate (Fig. 9).

The Medieval Warm Period (MWP) (ca. 1150–1300 AD)

Sedimentological and biological climate proxies characterize the period between the middle twelfth to beginning of the fourteenth centuries (units 6 and 5) as more arid than present. Gypsum formation and organic (algal) deposition indicate low lake levels and high water salinity, confirmed geochemically by more positive PCA2 values and by biological evidence (low diatom VC and the presence of *Campylodiscus clypeus* fragments (CF)). Pollen reflects warmer and drier conditions, with a landscape dominated by junipers, Mediterranean elements, a relatively low abundance of mesophylic woody taxa and a poorly developed aquatic component. High salinity and warmer climate would enhance stratification and long periods of anoxia on the lake bottom, as suggested by Prat et al. (1992) and Real et al. (2000), which favored the resistant chironomid species *Chironomus* (Brodersen et al. 2008). Nevertheless, during prolonged periods of anoxia, deep-water fauna is depauperated and the subfossil chironomid assemblage often becomes dominated by littoral taxa (Walker et al. 1991). Variable, but generally high clastic input indicates relatively enhanced erosion and runoff in the watershed. Although the presence of cultivated plants is clear, the low percentages indicate minimal

human pressure in the landscape. Parallel changes between cultivated plants and mesic woody taxa during this period suggest climatic control on farming activities, which increased when environmental conditions were more favorable (Fig. 9).

During the second half of the thirteenth century (~1250–1300 AD), deposition of fine clays may be related to top-soil erosion, following burning. Anoxic conditions in deep water might result from disturbances in the aquatic environment triggered by fire, as in modern environments (Vila-Escalé et al. 2007). Both sedimentological and palynological evidence supports the occurrence of fires in the watershed during this period, likely as a consequence of wars and/or deforestation for farming practices after the conquest of the territory by the Aragon Kingdom. Riera et al. (2006) also found a significant change in lake dynamics associated with an increase in charcoal concentration and proposed a change in the trophic status of the lake after 1,220 years AD due to forest clearance and farming activities.

In the IP, evidence of higher temperatures (Martínez-Cortizas et al. 1999) and decreased flooding activity, except the period 1160–1210 in the Tagus River watershed (Benito et al. 2003b), has been documented during medieval times. In southern Spain (Lake Zoñar, Andalusia), an arid phase occurred during the MWP (Martín-Puertas et al. 2008). In the Western Mediterranean region, higher sea surface temperatures (SST) (Taricco et al. 2008) and more arid conditions in continental areas (Magny et al. 2008) characterized this period. The Lake Estanya record is consistent with global reconstructions (Crowley and Lowery 2000; Osborn and Briffa 2006) that clearly document warmer conditions from the twelfth to fourteenth centuries, likely related to increased solar irradiance (Bard et al. 2000), persistent La Niña-like tropical Pacific conditions, a warm phase of the Atlantic Multidecadal Oscillation, and a more frequent positive phase of the North Atlantic Oscillation (Seager et al. 2007). The Estanya record also demonstrates more arid conditions in Mediterranean regions and southern Europe, in opposition to some evidence of a wet Medieval period in Scotland (Proctor et al. 2002).

The Little Ice Age (LIA) (ca. 1300–1850 AD)

The onset of the LIA in the Lake Estanya sequence is marked by the first evidence of increased water availability ca. 1300 AD: deposition of laminated facies D (subunit 4c), decrease in carbonates and gypsum content and an increase of riparian and HH, with the presence of *Potamogeton, Myriophyllum, Lemna* and *Nuphar*. This rise in lake level is accompanied by a recovery of both mesic woody taxa and cultivated plants during the fourteenth century. According to historical sources (Salrach 1995; Ubieto 1989), the increasing production of cereals, grapes and olives is contemporaneous with a rise in population in the region. At the onset of the Low Medieval crisis (Lacarra 1972; Riera et al. 2004), in the second half of the fourteenth century, this period of agricultural development ended. This was a period of large hydrological fluctuation, with the return of gypsum and organic-rich sediments (facies G), indicative of shallower and more chemically concentrated waters, during ca. 1340–1380 AD, as indicated by higher PCA2, and a positive excursion of $\delta^{18}O_{calcite}$. The reappearance of CF and the geochemical proxies (PCA2) also support this increase in salinity, suggesting generally shallow and fluctuating lake levels during the mid-late fourteenth century. At a global scale, some hydrological fluctuations indicative of the onset of the LIA, also occurred around 1300 AD (Denton and Broecker 2008).

A definitive, large hydrological change occurred in Lake Estanya at around 1380 AD. The end of gypsum precipitation at the top of unit 4b, the onset of deposition of laminated facies D (subunit 4a) parallel to a progressively decreasing trend in PCA2 are synchronous with an increase in diatom VC and species assemblages suggesting less concentrated waters (*C. distinguenda*, *Fragilaria brevistriata* and *Mastogloia smithii*) and to C:P > 1, reflecting the dominance of pelagic environments in the basin associated with relatively higher lake levels. The greater presence of littoral chironomid species could be explained as a reflection of higher habitat heterogeneity. An increase in HH pollen also occurred at this time. Regional vegetation shows the onset of the cold conditions that characterize the LIA and it is marked by better development of pines, mainly composed by the *Pinus nigra-sylvestris* type, and the decrease both of mesophilic trees (deciduous *Quercus* drop and disappearance of *Corylus, Tilia*) and thermophilic elements (evergreen *Quercus, Buxus, Viburnum* and disappearance of *Thymelaea*). Although farming activities and irrigation structures

(canals) could have had an impact on the hydrology of the lake, this period also shows a decrease in cultivated plants, indicating less human impact, and consequently points to climatically-induced changes in the lake.

Within this main humid and cold period (late fourteenth and early fifteenth centuries) short-lived arid phases occurred. Particularly at the beginning of the fifteenth century up to ca. 1440 AD, lower hydrological balance is indicated by: (1) the abundance of *Cocconeis placentula*, an epiphytic and epipelic diatom species, and *M. smithii*; (2) the marked increase of the hygrophyte component of the total HH and (3) the positive excursion in $\delta^{18}O_{calcite}$ reflecting an extension of littoral, carbonate-producing environments, related to the establishment of a more productive carbonate lacustrine shelf associated with a shallower lake. The marked decrease in both mesic and Mediterranean woody taxa and cultivated plants, parallel to the increase in *Pinus* and *Alnus* during the lower half of subunit 4a reflects a short crisis that, according to our chronological model, could be coincident with the Spörer minimum in solar irradiance and a cold phase of the LIA. The absence of diatoms after ca. 1450 AD indicates the return of adverse conditions for their survival or preservation.

At a global scale, the lower temperatures of the LIA after the fourteenth century (Mann et al. 1999; Moberg et al. 2005) coincided with colder North Atlantic (Bond et al. 2001) and Mediterranean SSTs (Taricco et al. 2008) and a phase of mountain glacier advance (Wanner et al. 2008). In the IP, generalized lower temperatures (Martínez-Cortizas et al. 1999) characterize this period. In spite of the lack of evidence of drastic changes in rainfall variability in NE Spain (Saz Sánchez 2003), the occurrence of lower summer temperatures, and thus, reduced evapotranspiration, likely generated moister conditions in the Mediterranean Basin (Luterbacher et al. 2005). This humid and cold phase recorded in Lake Estanya from the late fourteenth century until the beginning of the fifteenth century coincides with a first relative maximum of mountain glacier advance (Denton and Broecker 2008) and more humid conditions (Trachsel et al. 2008) in Central Europe. Both dendroclimatological reconstructions (Creus Novau et al. 1996) and lake records (Domínguez-Castro et al. 2006) show the occurrence of short abrupt hydrological fluctuations in N Spain during the fifteenth century, thus supporting our findings of a complex and variable LIA. Although harsh climates also could have been a factor, the decrease in cultivated areas corresponds to a period of economic crisis and depopulation in the region (Lacarra 1972).

A third phase of higher lake levels and more humid conditions occurred after ca. 1530 AD and lasted up to ca. 1750 AD. The deposition of massive facies C, the low PCA2 values, the negative excursion of $\delta^{18}O_{calcite}$, the abrupt shift towards more negative $\delta^{13}C_{org}$ and the increase in clastic input, all are indicative of enhanced runoff, higher water availability and more dilute waters. Diatom abundance and presence of pelagic species are also coherent with higher lake levels. The significant change in chironomid assemblages points to the development of more littoral environments, enhanced by the flooding of the shallower areas. Based on pollen and sedimentological evidence, Riera et al. (2004, 2006) reconstructed the highest water level in Lake Estanya during the period ~1500–1580 AD. According to our reconstruction, a lake level rise took place during the sixteenth century, but the highest level occurred later (Fig. 9). This increase in water availability during the sixteenth century coincides with higher AP content, with a marked increase of deciduous oak, among other mesophilic trees, indicative of climatic amelioration. More common facies D and increased clastic input indicate that the period between ca. 1650 and ca. 1750 (subunit 3a) has the highest soil erosion rates of the whole sequence (Figs. 4, 9). This period corresponds to an increase in cultivated pollen taxa and, according to documentary data (Lacarra 1972), to increasing population in the area. A brief period of lower water levels and increased salinity occurred at the turn of the eighteenth century (~1750–1800 AD, transition to unit 2), marked by the reappearance of CF (Fig. 7), a slight but significant reduction of HH, and changes in chironomid assemblages (Fig. 9).

Moister conditions on the IP during this phase of the LIA (1500–1750 AD) are documented by the increase in flood frequency in the Tagus River watershed (Benito et al. 2003a; Moreno et al. 2008), reaching maximum frequency and intensity during the sixteenth century, and archaeological records (Ferrio et al. 2006) in the Ebro Basin. The occurrence of arid conditions during the late eighteenth century correlates with the so-called Maldá

Anomaly in NE Spain (Barriendos and Llasat 2003), a period characterized by strong climate variability and the occurrence of both catastrophic floods and severe aridity crises in nearby Catalonia.

One of the most significant hydrological, vegetation and depositional changes of the last millennium occurred in Lake Estanya during the transition to the nineteenth century. It was characterized by a marked increase in water availability and the development of a larger and deeper lake, leading to the deposition of laminated facies B, a decreasing clastic input, a higher contribution of the littoral carbonate shelf to the sediments and the onset of more frequent anoxic hypolimnetic conditions. This change correlates with a drastic increase in organic productivity recorded by diatoms (higher BSi and VC) and chironomid HC, contemporaneous with a higher abundance and diversity of HH (both riparian trees and hygrophytes in littoral areas and hydrophytes in pelagic environments). Higher diatom C:P ratios, resulting from the abundance of *Cyclotella distinguenda*, also support this interpretation. The terrestrial vegetation component also indicates more humid conditions with the maintenance of similar proportions of mesophytes and the establishment of a landscape similar to the present one. The $\delta^{18}O_{calcite}$ values remain low and start increasing towards the top, coinciding with higher carbonate content, and likely related to the precipitation of calcite in littoral areas. Although evidence of increased water management at this time has been documented (Riera et al. 2004, 2006), the contribution of the artificial canals connecting the three lakes can be considered negligible compared to the estimated increase in lake level. This hydrological change coincides with the absolute maximum of cultivars throughout the sequence, reflecting the maximum expansion of agriculture in the area—and in general in the mountain areas of the Pyrenees (Fillat et al. 2008) during the nineteenth century. The mid-nineteenth century *Olea* peak was also documented by Riera et al. (2004). The development of meromixis in Lake Estanya during this period might have been a response to processes similar to those described in another Iberian, deep karstic lake (La Cruz, Iberian Range) as a result of the synergistic effects of cold phases of the LIA and intense human impact in the watershed, leading to higher lake levels and trophic status (Julià et al. 1998). Dendroclimatological reconstructions for NE Spain (Saz Sánchez 2003) and available IP lake records show some evidence of humid conditions during the late nineteenth century [e.g. Lake Zoñar (Martín-Puertas et al. 2008); Lake Taravilla (Moreno et al. 2008); Archidona (Luque et al. 2004)], likely explained by reduced evaporation and higher winter precipitation.

From the end of the Little Ice Age to the present (ca. 1850–2004 AD)

A general decrease in cultivated plants occurred during the late nineteenth century. The marked reduction in *Olea* might be related to destruction of olive trees by frost around 1887 AD (Riera et al. 2004; Salrach 1995), and the depopulation of the area during that period. The late nineteenth century witnessed the last cold spell of the LIA, characterized by a new episode of glacier advance in the Alps and a recovery of water level in alpine lakes (Magny et al. 2008). The reduction in siliciclastic input to the lake during the upper part of unit 2 was a consequence of both climate and human factors: relatively higher lake levels and the buffer effect of littoral vegetation, as well as a reduction of anthropogenic pressure in the watershed. The higher carbonate content of pelagic sediments was caused by better development of calcite-producing littoral areas, as recorded by the more positive PCA2 and $\delta^{18}O_{calcite}$ values. A general trend to slightly lower lake levels during the twentieth century is suggested by the loss of lamination of the sediments and the abundance of more littoral species of chironomids and epiphytic diatoms. Decreased rainfall during the mid to late twentieth century in the area (Saz Sánchez 2003), warmer global temperatures (Mann and Jones 2003) and thus, higher evaporation, might explain this trend. Other wetlands from the IP have recorded relatively less humid conditions after the end of the LIA [e.g. Lake Zoñar, (Martín-Puertas et al. 2008); Doñana, (Sousa and García-Murillo 2003)].

After the mid twentieth century (transition between units 2 and 1) the deposition of massive facies A suggests a decrease in anoxia and shallower conditions. Increased carbonate production, reflected both by mineralogical and geochemical indicators, and decreased organic productivity coincident with enhanced terrestrial organic matter input, characterized this last period. The decline in VC and the appearance of species such as *Cymbella amphipleura*

also suggest a decrease in lake level. The increase in LSR during the last 40 years (average of 3.7 mm/year, Fig. 3) is caused by higher input of littoral carbonate particles to the deeper areas rather than to increased siliciclastic transport from the watershed, as shown by the XRF data (Fig. 5). Farming in the watershed (cereal crops) is the main factor controlling the recent intense catchment erosion and soil loss (estimated as 5.38 Mg ha^{-1} $year^{-1}$) and consequent high sediment load transported to the lake (López-Vicente et al. 2008). Farmland abandonment, related to the loss of population in the region during the period 1960–1980 AD, could explain the changes in sediment accumulation detected with ^{210}Pb dating. Reduced anthropogenic impact in the lake watershed may have been conducive to better conditions (less turbidity) for the development of littoral environments. During the last 40 years, an increase in epiphytic diatoms coincides with the expansion of charophytes (Riera et al. 2004) and Chironomidae species *Ablabesmyia longistyla* or *Dicrotendipes modestus* (Álvarez Cobelas and Cirujano 2007).

Concluding remarks

A comparison of the main hydrological transitions during the last 800 years in Lake Estanya and solar irradiance (Bard et al. 2000) reveals that lower lake levels dominated during periods of enhanced solar activity (MWP and post—ca. 1850 AD) and higher lake levels during periods of diminished solar activity (LIA). A similar pattern has been documented in other high-resolution, multiproxy lake records in southern Spain [Zoñar (Martín-Puertas et al. 2008)] and in the Alps (Magny et al. 2008). In Lake Estanya, periods of rapidly decreasing water level or generally lower water table lie within phases of maximum solar activity (Fig. 9): (1) the MWP, (2) ~1340–1380 AD (unit 4B); (3) the ~1470–1490 AD (transition 4A–3B), (4) ca. 1770 AD (transition subunits 3a–2), (5) post ca. 1850 AD. Periods of higher lake levels or evidence of increased water balance in the basin occurred during the solar minima of Wolf (1282–1342 AD), (onset of the LIA), Sporer (1460–1550 AD, transition subunit 4a–3b), Maunder (1645–1715 AD), subunit 3a and Dalton (1790–1830 AD, lower half of subunit 2).

The paleohydrological reconstruction from Lake Estanya shows more similarities with southern Europe (Zoñar (Martín-Puertas et al. 2008), the Azores (Björck et al. 2006) and alpine [Lake Joux (Magny et al. 2008)] lake records than with high latitude, northern European ones [Lake Nautajärvi (Ojala and Alenius 2005); and Lake Korttajärvi (Tiljander et al. 2003)]. Particularly, the humid phase at 300–400 cal year BP (1540–1700 AD) in the Azores and Joux corresponds to a large lake level increase in Zoñar lake in the sixteenth century and with a significant humid period in Lake Estanya. Although generally colder conditions during the LIA may have had an impact on lower evaporation rates in Mediterranean areas during the summer months, the large increase in aquifer recharge indicated by proxies points to increases in annual rainfall, which most likely occurred during winter. Such a humidity increase in southern latitudes could be related to strengthening of the westerlies (Björck et al. 2006). A dominance of negative NAO phases during the LIA could also account for the different paleohydrological response between northern and southern European records.

Acknowledgments This research was funded through the projects LIMNOCAL (CGL2006-13327-C04-01), PALEODIVERSITAS (CGL2006-02956/BOS), GRACCIE (CSD2007-00067) supported by the Spanish Inter-Ministry Commission of Science and Technology (CICYT); and PM073/2007 provided by the Diputación General de Aragón. The Aragonese Regional Government and CAJA INMACULADA provided two travel grants for the analyses carried out at Univ. of Cádiz and EEZ-CSIC (Spain), and MARUM Centre (Univ. of Bremen, Germany). M. Morellón was supported by a PhD contract with the CONAI + D (Aragonese Scientific Council for Research and Development). We are indebted to Anders Noren, Doug Schnurrenberger and Mark Shapley (LRC-University of Minnesota) for the 2004 coring campaign and Santiago Giralt and Armand Hernández (IJA-CSIC), as well as Alberto Sáez and J.J. Pueyo-Mur (University of Barcelona) for coring assistance in 2006. We also acknowledge Cristina Pérez Bielsa (IGME) for her help in water and short-core sampling, Joan Gomà and Roger Flower for their help with the identification of diatom species, and Marco Klann (MARUM Centre, Univ. of Bremen) for biogenic silica analyses. We are also grateful to EEZ-CSIC, EEAD-CSIC and IPE-CSIC laboratory staff for their collaboration in this research. We thank Dirk Verschuren and Santiago Giralt for their helpful comments and their criticism, which led to a considerable improvement of the manuscript.

References

Aboal M, Álvarez-Cobelas M, Cambra J, Ector L (2003) Floristic list of the non marine diatoms (Bacillariophyceae) of Iberian Peninsula, Balearic Islands and Canary Islands.

A.R.G. Witkowski A., Gantner Verlag K.G., FL 9491, Ruggell

Abrantes F, Gil I, Lopes C, Castro M (2005) Quantitative diatom analyses: a faster cleaning procedure. Deep Sea Res 52:189–198. doi:10.1016/j.dsr.2004.05.012

Álvarez Cobelas M, Cirujano S (2007) Ecología acuática y sociedad de las Lagunas de Ruidera. Consejo Superior de Investigaciones Científicas (C.S.I.C.), Madrid, Spain, 414 pp

Álvarez MC, Flores JA, Sierro FJ, Diz P, Francès G, Pelejero C, Grimalt JO (2005) Millennial surface water dynamics in the Ría de Vigo during the last 3000 years as revealed by coccoliths and molecular biomarkers. Palaeogeogr Palaeoclimatol Palaeoecol 218:1–13. doi:10.1016/j.palaeo.2004.12.002

Appleby PG (2001) Chronostratigraphic techniques in recent sediments. In: Last WM, Smol JP (eds) Tracking environmental change using lake sediments volume 1: basin analysis, coring, and chronological techniques. Kluwer, Dordrecht, pp 171–203

Ávila A, Burrel JL, Domingo A, Fernández E, Godall J, Llopart JM (1984) Limnología del Lago Grande de Estanya (Huesca). Oecol Aquat 7:3–24

Bard E, Frank M (2006) Climate change and solar variability: what's new under the sun? Earth Planet Sci Lett 248:1–14. doi:10.1016/j.epsl.2006.06.016

Bard E, Raisbeck G, Yiou F, Jouzel J (2000) Solar irradiance during the last 1200 years based on cosmogenic nuclides. Tellus B Chem Phys Meterol 52:985–992. doi:10.1034/j.1600-0889.2000.d01-7.x

Barriendos M, Llasat MC (2003) The case of the 'Maldá' anomaly in the Western Mediterranean Basin (AD 1760–1800): an example of a strong climatic variability. Clim Change V61:191–216. doi:10.1023/A:1026327613698

Battarbee RW (1986) Diatom analysis. In: Berglund BE (ed) Handbook of holocene palaeoecology and palaeohydrology. Wiley, Chichester, pp 527–570

Battarbee RW, Jones V, Flower RJ, Cameron NG, Bennion H, Carvalho L, Juggins S (2001) Diatoms. In: Smol JP, Birks HJB, Last WM (eds) Tracking environmental change using lake sediments. Kluwer, Dordrecht

Benito G, Díez-Herrero A, Fernández de Villalta M (2003a) Magnitude and frequency of flooding in the Tagus Basin (Central Spain) over the last millennium. Clim Change 58:171–192. doi:10.1023/A:1023417102053

Benito G, Sopeña A, Sánchez-Moya Y, Machado MJ, Pérez-González A (2003b) Palaeoflood record of the Tagus River (Central Spain) during the Late Pleistocene and Holocene. Quat Sci Rev 22:1737–1756. doi:10.1016/S0277-3791(03)00133-1

Bennet K (2002) Documentation for Psimpoll 4.10 and Pscomb 1.03. C programs for plotting pollen diagrams and analysing pollen data. University of Cambridge, Cambridge

Björck S, Rittenour T, Rosén P, França Z, Möller P, Snowball I, Wastegard S, Bennikee O, Kromer B (2006) A Holocene lacustrine record in the central North Atlantic: proxies for volcanic activity, short-term NAO mode variability, and long-term precipitation changes. Quat Sci Rev 25:9–32. doi:10.1016/j.quascirev.2005.08.008

Bond G, Kromer B, Beer J, Muscheler R, Evans MN, Showers W, Hoffman S, Lotti-Bond R, Hajdas I, Bonani G (2001) Persistent solar influence on North Atlantic climate during the Holocene. Science 294:2130–2136. doi:10.1126/science.1065680

Bradley RS, Hughes MK, Diaz HF (2003) Climate change: climate in medieval time. Science 302:404–405. doi:10.1126/science.1090372

Brenner M, Whitmore TJ, Curtis JH, Hodell DA, Schelske CL (1999) Stable isotope (δ^{13}C and δ^{15}N) signatures of sedimented organic matter as indicators of historic lake trophic state. J Paleolimnol 22:205–221. doi:10.1023/A:1008078222806

Brodersen KP, Odgaard BV, Vestergaard O, Anderson NJ (2001) Chironomid stratigraphy in the shallow and eutrophic Lake Søbygaard, Denmark: chironomid-macrophyte co-occurrence. Freshw Biol 46:253–267. doi:10.1046/j.1365-2427.2001.00652.x

Brodersen KP, Pedersen OLE, Walker IANR, Jensen MT (2008) Respiration of midges (Diptera; Chironomidae) in British Columbian lakes: oxy-regulation, temperature and their role as palaeo-indicators. Freshw Biol 53:593–602. doi:10.1111/j.1365-2427.2007.01922.x

Brooks SJ, Langdon PG, Heiri O (2007) The identification and use of palaearctic Chironomidae larvae in palaeoecology. ORA technical guide no. 10. Quaternary Research Association Technical Guide, 276 pp

Chung FH (1974a) Quantitative interpretation of X-ray diffraction patterns of mixtures. I. Matrix-flushing method for quantitative multicomponent analysis. J Appl Crystallogr 7:519–525

Chung FH (1974b) Quantitative interpretation of X-ray diffraction patterns of mixtures. II. Adiabatic principle of X-ray diffraction analysis of mixtures. J Appl Crystallogr 7:526–531

Cohen AS (2003) Paleolimnology: the history and evolution of lake systems. Oxford University Press, New York, p 500

Cohn M, Urey HC (1938) Oxygen exchange reactions of organic compounds and water. J Am Chem Soc 60:679–687. doi:10.1021/ja01270a052

Colman SM, Peck JA, Karabanov EB, Carter SJ, Bradbury JP, King JW, Williams DF (1995) Continental climate response to orbital forcing from biogenic silica records in Lake Baikal. Nature 378:769–771. doi:10.1038/378769a0

Cooper SR (1995) Chesapeake Bay watershed historical land use: impact on water quality and diatom communities. Ecol Appl 5:703–723. doi:10.2307/1941979

Creus Novau J, Fernández Cancio A, Manrique Menéndez E (1996) Evolución de la temperatura y la precipitación anuales desde el año 1400 en el sector central de la Depresión del Ebro. Luc Mall 8:9–27

Crowley TJ, Lowery TS (2000) How warm was the Medieval Warm Period? Ambio 29:51–54

Davis BAS (1994) Paleolimnology and Holocene environmental change from endorheic lakes in the Ebro Basin, north-east Spain. University of Newcastle upon Tyne, p 317

De Master DJ (1981) The supply and accumulation of silica in the marine environment. Geochim Cosmochim Acta 32:1128–1140

Denton GH, Broecker WS (2008) Wobbly ocean conveyor circulation during the Holocene? Quat Sci Rev 27:1939–1950. doi:10.1016/j.quascirev.2008.08.008

Desprat S, Sánchez Goñi MF, Loutre M-F (2003) Revealing climatic variability of the last three millennia in northwestern Iberia using pollen influx data. Earth Planet Sci Lett 213:63–78. doi:10.1016/S0012-821X(03)00292-9

Domínguez-Castro F, Santisteban JI, Mediavilla R, Dean WE, López-Pamo E, Gil-García MJ, Ruiz-Zapata MB (2006) Environmental and geochemical record of human-induced changes in C storage during the last millennium in a temperate wetland (Las Tablas de Daimiel National Park, central Spain). Tellus B Chem Phys Meterol 58:573–585. doi:10.1111/j.1600-0889.2006.00211.x

Dupré M (1992) Palinología. Sociedad Española de Geomorfología, 30 pp

Engstrom DR, Schottler SP, Leavitt PR, Havens KE (2006) A reevaluation of the cultural eutrophication of lake Okeechobee using multiproxy sediment records. Ecol Appl 16:1194–1206. doi:10.1890/1051-0761(2006)016[1194:AROTCE]2.0.CO;2

Epstein S, Mayeda TK (1953) Variation of the $^{18}O/^{16}O$ ratio in natural waters. Geochim Cosmochim Acta 4:213–224. doi:10.1016/0016-7037(53)90051-9

Esteban-Amat E (2003) La humanización de las altas cuencas de la Garona y las Nogueras (4500 AC–1955 DC). Ministerio de Medio Ambiente, Secretaría General de Medio Ambiente, Organismo Autónomo de Parques Nacionales, Madrid

Ferrio JP, Alonso N, López JB, Araus JL, Voltas J (2006) Carbon isotope composition of fossil charcoal reveals aridity changes in the NW Mediterranean Basin. Glob Change Biol 12:1253–1266. doi:10.1111/j.1365-2486.2006.01170.x

Fillat F, García-González R, Gómez D, Reiné R (2008) Pastos del Pirineo. Consejo Superior de Investigaciones Científicas (C.S.I.C.), Madrid, Spain, 319 pp

Fischer H, Werner M, Wagenbach D, Schwager M, Thorsteinnson T, Wilhelms F, Kipfstuhl J, Sommer S (1998) Little Ice Age clearly recorded in northern Greenland ice cores. Geophys Res Lett 25:1749–1752. doi:10.1029/98GL01177

Flower RJ (1993) Diatom preservation: experiments and observations on dissolution and breakage in modern and fossil material. Hydrobiologia 269–270:473–484. doi:10.1007/BF00028045

Gil García M, Ruiz Zapata M, Santisteban J, Mediavilla R, López-Pamo E, Dabrio C (2007) Late holocene environments in Las Tablas de Daimiel (south central Iberian peninsula, Spain). Veg Hist Archaeobot 16:241–250. doi:10.1007/s00334-006-0047-9

Giralt S, Moreno A, Bao R, Sáez A, Prego R, Valero-Garcés B, Pueyo J, González-Sampériz P, Taberner C (2008) A statistical approach to disentangle environmental forcings in a lacustrine record: the Lago Chungará case (Chilean Altiplano). J Paleolimnol 40:195–215. doi:10.1007/s10933-007-9151-9

Griffiths SJ, Street-Perrott FA, Holmes JA, Leng MJ, Tzedakis C (2002) Chemical and isotopic composition of modern water bodies in the Lake Kopais Basin, central Greece: analogues for the interpretation of the lacustrine sedimentary sequence. Sediment Geol 148:79–103. doi:10.1016/S0037-0738(01)00211-1

Guilaine J (1991) Pour une archéologie agraire. Armand Colin, Paris

IGME (1982) Mapa Geológico de España 1:50000 No. 289. Benabarre. Instituto Geológico y Minero de España, Madrid

Jansen E, Overpeck J, Briffa KR, Duplessy J-C, Joos F, Masson-Delmotte V, Olago D, Otto-Bliesner B, Peltier WR, Rahmstorf S, Ramesh R, Raynaud D, Rind D, Solomina O, Villalba R, Zhang D (2007) Palaeoclimate. In: Climate Change 2007: the physical science basis. Intergovernmental Panel on Climate Change, Cambridge

Johnson TC, Barry SL, Chan Y, Wilkinson P (2001) Decadal record of climate variability spanning the past 700 year in the Southern Tropics of East Africa. Geology 29:83–86. doi:10.1130/0091-7613(2001)029≤0083:DROCVS≥2.0.CO;2

Jordán de Asso y del Río I (1798) Historia de la Economía Política de Aragón Zaragoza

Julià R, Burjachs F, Dasí MJ, Mezquita F, Miracle MR, Roca JR, Seret G, Vicente E (1998) Meromixis origin and recent trophic evolution in the Spanish mountain lake La Cruz. Aquat Sci 60:279–299. doi:10.1007/s000270050042

Kirov B, Georgieva K (2002) Long-term variations and interrelations of ENSO, NAO and solar activity. Phys Chem Earth 27:441–448

Krammer K (2002) Diatoms of Europe. Diatoms of the European Inland Waters and Comparable Habitats. A.R.G. Gantner Verlag K.G, Ruggell, p 584

Krammer K, Lange-Bertalot H (1986) Süsswasserßora von Mitteleuropa. Bacillariophyceae. 1. Teil: Naviculaceae. Gustav Fischer Verlag, Stuttgart, p 876

Lacarra JM (1972) Aragón en el pasado. Austral, Madrid

Lange-Bertalot H (2001) Diatoms of the Europe inland waters and comparable habitats. A.R.G. Gantner Verlag K.G., Ruggell, p 526

Last WM, Smol JP (2001) Tracking environmental change using lake sediments. Kluwer Academic Publishers, Norwell

Leng MJ, Marshall JD (2004) Palaeoclimate interpretation of stable isotope data from lake sediment archives. Quat Sci Rev 23:811–831. doi:10.1016/j.quascirev.2003.06.012

León-Llamazares A (1991) Caracterización agroclimática de la provincia de Huesca Ministerio de Agricultura, Pesca y Alimentación (M.A.P.A.), Madrid

López-Vicente M, Navas A, Machín J (2008) Identifying erosive periods by using RUSLE factors in mountain fields of the Central Spanish Pyrenees. Hydrol Earth Syst Sci 12:523–535

López-Vicente M, Navas A, Machín J (2009) Geomorphic mapping in endorheic catchments in the Spanish Pyrenees: an integrated GIS analysis of karstic features. Geomorphology. doi:10.1016/j.geomorph.2008.03.014

Luque JA, Julià R (2002) Lake sediment response to land-use and climate change during the last 1000 years in the oligotrophic Lake Sanabria (northwest of Iberian Peninsula). Sediment Geol 148:343–355. doi:10.1016/S0037-0738(01)00225-1

Luque JA, Julià R, Riera S, Marqués MA, López-Sáez JA, Mezquita F (2004) Respuesta sedimentológica a los cambios ambientales de épocas históricas en el sur de la

Península Ibérica: La secuencia de la Laguna Grande de Archidona (Málaga). Geotemas 6:113–116

Luterbacher J, Xoplaki E, Casty C, Wanner H, Pauling A, Küttel M, Rutishauser T, Brönnimann S, Fischer E, Fleitmann D, González-Rouco FJ, García-Herrera R, Barriendos M, Rodrigo F, Gonzalez-Hidalgo JC, Saz MA, Gimeno L, Ribera P, Brunet M, Paeth H, Rimbu N, Felis T, Jacobeit J, Dünkeloh A, Zorita E, Guiot J, Türkes M, Alcoforado MJ, Trigo R, Wheeler D, Tett S, Mann ME, Touchan R, Shindell DT, Silenzi S, Montagna P, Camuffo D, Mariotti A, Nanni T, Brunetti M, Maugeri M, De Zerefos C, Zolt S, Lionello P (2005) Mediterranean climate variability over the last centuries: a review. In: Lionello P, Malanotte-Rizzoli P, Boscolo R (eds) The Mediterranean climate: an overview of the main characteristics and issues. Elsevier, Amsterdam, pp 27–148

Magny M, Gauthier E, Vanniere B, Peyron O (2008) Palaeohydrological changes and human-impact history over the last millennium recorded at Lake Joux in the Jura Mountains, Switzerland. Holocene 18:255–265. doi:10.1177/0959683607086763

Mann ME, Jones PD (2003) Global surface temperatures over the past two millennia. Geophys Res Lett 30. doi:10.1029/2003GL017814

Mann ME, Bradley RS, Hughes MK (1999) Northern Hemisphere temperatures during the past millennium: inferences, uncertainties, and limitations. Geophys Res Lett 26:759–762. doi:10.1029/1999GL900070

Martínez-Cortizas A, Pontevedra-Pombal X, García-Rodeja E, Nóvoa Muñoz JC, Shotyk W (1999) Mercury in a Spanish Peat Bog: archive of climate change and atmospheric metal deposition. Science 284:939–942. doi:10.1126/science.284.5416.939

Martín-Puertas C, Valero-Garcés BL, Mata MP, González-Sampériz P, Bao R, Moreno A, Stefanova V (2008) Arid and humid phases in southern Spain during the last 4000 years: the Zoñar Lake record, Cordoba. Holocene 18:907–921. doi:10.1177/0959683608093533

McCrea JM (1950) On the isotopic chemistry of carbonates and a paleotemperature scale. J Chem Phys 18:849–857. doi:10.1063/1.1747785

Meyers PA, Lallier-Vergès E (1999) Lacustrine sedimentary organic matter records of Late Quaternary paleoclimates. J Paleolimnol 21:345–372. doi:10.1023/A:1008073732192

Moberg A, Sonechkin DM, Holmgren K, Datsenko NM, Karlen W (2005) Highly variable Northern Hemisphere temperatures reconstructed from low- and high-resolution proxy data. Nature 433:613–617. doi:10.1038/nature03265

Moore PD, Webb JA, Collinson ME (1991) Pollen analysis. Blackwell, Oxford

Morellón M, Valero-Garcés B, Moreno A, González-Sampériz P, Mata P, Romero O, Maestro M, Navas A (2008) Holocene palaeohydrology and climate variability in Northeastern Spain: the sedimentary record of Lake Estanya (Pre-Pyrenean range). Quat Int 181:15–31. doi:10.1016/j.quaint.2007.02.021

Morellón M, Valero-Garcés BL, Anselmetti F, Ariztegui D, Schnellmann M, Moreno A, Mata P, Rico M, Corella JP (2009) Late Quaternary deposition and facies model for karstic Lake Estanya (NE Spain). Sedimentology. doi:10.1111/j.1365-3091.2008.01044.x

Moreno A, Valero-Garcés BL, González-Sampériz P, Rico M (2008) Flood response to rainfall variability during the last 2000 years inferred from the Taravilla Lake record (Central Iberian Range, Spain). J Paleolimnol 40:943–961. doi:10.1007/s10933-008-9209-3

Müller PJ, Schneider R (1993) An automated leaching method for the determination of opal in sediments and particulate matter. Deep Sea Res Part I Oceanogr Res Pap 40:425–444. doi:10.1016/0967-0637(93)90140-X

Muller J, Kylander M, Martínez-Cortizas A, Wüst RAJ, Weiss D, Blake K, Coles B, García-Sanchez R (2008) The use of principle component analyses in characterising trace and major elemental distribution in a 55 kyr peat deposit in tropical Australia: implications to paleoclimate. Geochim Cosmochim Acta 72:449–463. doi:10.1016/j.gca.2007.09.028

Ojala AEK, Alenius T (2005) 10 000 years of interannual sedimentation recorded in the Lake Nautajärvi (Finland) clastic-organic varves. Palaeogeogr Palaeoclimatol Palaeoecol 219:285–302. doi:10.1016/j.palaeo.2005.01.002

Osborn TJ, Briffa KR (2006) The spatial extent of 20th-century warmth in the context of the past 1200 years. Science 311:841–844. doi:10.1126/science.1120514

Peinado Lorca M, Rivas-Martínez S (1987) La vegetación de España, 544 pp

Prat N, Rieradevall M (1995) Life cycle and production of Chironomidae (Diptera) from Lake Banyoles (NE Spain). Freshw Biol 33:511–524. doi:10.1111/j.1365-2427.1995.tb00410.x

Prat N, Real M, Rieradevall M (1992) Benthos of Spanish lakes and reservoirs. Limnetica 8:221–230

Proctor CJ, Baker A, Barnes WL (2002) A three thousand year record of North Atlantic climate. Clim Dyn 19:449–454. doi:10.1007/s00382-002-0236-x

Real M, Rieradevall M, Prat N (2000) *Chironomus* species (Diptera: Chironomidae) in the profundal benthos of Spanish reservoirs and lakes: factors affecting distribution patterns. Freshw Biol 43:1–18. doi:10.1046/j.1365-2427.2000.00508.x

Reimer PJ, Baillie MGL, Bard E, Bayliss A, Beck JW, Bertrand CJH, Blackwell PG, Buck CE, Burr GS, Cutler KB, Damon PE, Edwards RL, Fairbanks RG, Friedrich M, Guilderson TP, Hogg AG, Hughen KA, Kromer B, McCormac G, Manning S, Ramsey CB, Reimer RW, Remmele S, Southon JR, Stuiver M, Talamo S, Taylor FW, van der Plicht J, Weyhenmeyer CE (2004) IntCal04 terrestrial radiocarbon age calibration, 0–26 Cal Kyr BP. Radiocarbon 46:1029–1058

Richter TO, Van der Gaast SJ, Koster B, Vaars AJ, Gieles R, De Stigter HC, De Haas H, Van Weering TCE (2006) The Avaatech XRF Core Scanner: technical description and applications to NE Atlantic sediments. In: Rothwell RG (ed) New techniques in sediment core analysis. The Geological Society of London, London, pp 39–50

Riera S, Wansard R, Julià R (2004) 2000-year environmental history of a karstic lake in the Mediterranean Pre-Pyrenees: the Estanya Lakes (Spain). Catena 55:293–324. doi:10.1016/S0341-8162(03)00107-3

Riera S, López-Sáez JA, Julià R (2006) Lake responses to historical land use changes in northern Spain: the

contribution of non-pollen palynomorphs in a multiproxy study. Rev Palaeobot Palynol 141:127–137. doi:10.1016/j.revpalbo.2006.03.014

Rieradevall M, Brooks SJ (2001) An identification guide to subfossil Tanypodinae larvae (Insecta: Diptera: Chironomidae) based on cephalic setation. J Paleolimnol 25:81–99. doi:10.1023/A:1008185517959

Risberg J, Alm G, Goslar T (2005) Variable isostatic uplift patterns during the Holocene in southeast Sweden, based on high-resolution AMS radiocarbon datings of lake isolations. Holocene 15:847–857. doi:10.1191/0959683605hl858ra

Rivas-Martínez S (1982) Étages bioclimatiques, secteurs chorologiques et séries de végetation de l'Espagne méditerranéenne. Ecol Medit VIII:275–288

Romero-Viana L, Julià R, Camacho A, Vicente E, Miracle M (2008) Climate signal in varve thickness: Lake La Cruz (Spain), a case study. J Paleolimnol 40:703–714. doi:10.1007/s10933-008-9194-6

Ruas M-P (1990) Analyse des paléo-semences carbonisées. In: Raynaud C (ed) Le village gallo-romain et médiéval de Lunel-Viel (Hérault) La fouille du quartier ouest (1981–1983). Centre de Recherches d'Histoire Ancienne, pp 96–104

Saether OA (1979) Chironomid communities as water quality indicators. Ecography 2:65–74. doi:10.1111/j.1600-0587.1979.tb00683.x

Salrach JM (1995) La formació de la societat feudal. Ss. VI–XII. Història, Política, Societat i Cultura dels Països Catalans. Grup Enciclopèdia Catalana, Barcelona

Sancho-Marcén C (1988) El Polje de Saganta (Sierras Exteriores pirenaicas, prov. de Huesca). Cuat Geomorf 2:107–113

Saros JE, Fritz SC, Smith AJ (2000) Shifts in mid- to late-Holocene anion composition in Elk Lake (Grant County, Minnesota): comparison of diatom and ostracode inferences. Quat Int 67:37–46. doi:10.1016/S1040-6182(00)00007-0

Saz Sánchez MA (2003) Temperaturas y precipitaciones en la mitad norte de España desde el siglo XV. Estudio Dendroclimático. Publicaciones del Consejo de la Naturaleza de Aragón, Zaragoza

Schmid PE (1993) A key to the larval Chironomidae and their instars from Austrian Danube region streams and rivers with particular reference to a numerical taxonomic approach. Part I. Diamesinae, Prodiamesinae and Orthocladiinae. Wasser Abwasser Supplement 3:1–514

Schnurrenberger D, Russell J, Kelts K (2003) Classification of lacustrine sediments based on sedimentary components. J Paleolimnol 29:141–154. doi:10.1023/A:1023270324800

Seager R, Graham N, Herweijer C, Gordon AL, Kushnir Y, Cook E (2007) Blueprints for Medieval hydroclimate. Quat Sci Rev 26:2322–2336. doi:10.1016/j.quascirev.2007.04.020

Shindell DT, Schmidt GA, Mann ME, Rind D, Waple A (2001) Solar forcing of regional climate change during the Maunder minimum. Science 294:2149–2152. doi:10.1126/science.1064363

Smol J (1995) Paleolimnological aproaches to the evaluation and monitoring of ecosystem health: providing a history for environmental damage and recovery. In: Rapport D, Gaudet L, Calow P (eds) Evaluating and monitoring the health of large-scale ecosystems. Springer-Verlag, Berlin, pp 301–318

Sousa A, García-Murillo P (2003) Changes in the Wetlands of Andalusia (Doñana Natural Park, SW Spain) at the end of the Little Ice Age. Clim Change 58:193–217. doi:10.1023/A:1023421202961

Stockmarr J (1971) Tables with spores used in absolute pollen analysis. Pollen Spores 13:614–621

Talbot MR (1990) A review of the palaeohydrological interpretation of carbon and oxygen isotopic ratios in primary lacustrine carbonates. Chem Geol Isotope Geosci Sect 80:261–279

Taricco C, Ghil M, Vivaldo G (2008) Two millennia of climate variability in the Central Mediterranean. Clim Past Discuss 4:1089–1113

Tiljander M, Saarnisto M, Ojala AEK, Saarinen T (2003) A 3000-year palaeoenvironmental record from annually laminated sediment of Lake Korttajarvi, central Finland. Boreas 32:566–577. doi:10.1080/03009480310004152

Trachsel M, Eggenberger U, Grosjean M, Blass A, Sturm M (2008) Mineralogy-based quantitative precipitation, temperature reconstructions from annually laminated lake sediments (Swiss Alps) since AD 1580. Geophys Res Lett 35:L13707. doi:10.1029/2008GL034121

Ubieto A (1989) Historia de Aragón. Anubar, Zaragoza

Valero Garcés BL, Moreno A, Navas A, Mata P, Machín J, Delgado Huertas A, González Sampériz P, Schwalb A, Morellón M, Cheng H, Edwards RL (2008) The Taravilla lake and tufa deposits (Central Iberian Range, Spain) as palaeohydrological and palaeoclimatic indicators. Palaeogeogr Palaeoclimatol Palaeoecol 259:136–156. doi:10.1016/j.palaeo.2007.10.004

Valero-Garcés B, Navas A, Machín J, Stevenson T, Davis B (2000) Responses of a Saline Lake ecosystem in a semi-arid region to irrigation and climate variability: the history of Salada Chiprana, Central Ebro Basin, Spain. Ambio 29:344–350

Valero-Garcés B, González-Sampériz P, Navas A, Machín J, Mata P, Delgado-Huertas A, Bao R, Moreno A, Carrión JS, Schwalb A, González-Barrios A (2006) Human impact since medieval times and recent ecological restoration in a Mediterranean lake: the Laguna Zoñar, southern Spain. J Paleolimnol 35:441–465. doi:10.1007/s10933-005-1995-2

Verschuren D, Tibby J, Sabbe K, Roberts N (2000) Effects of depth, salinity, and substrate on the invertebrate community of a fluctuating tropical lake. Ecology 81:164–182

Vila-Escalé M, Vegas-Vilarrúbia T, Prat N (2007) Release of polycyclic aromatic compounds into a Mediterranean creek (Catalonia, NE Spain) after a forest fire. Water Res 41:2171–2179. doi:10.1016/j.watres.2006.07.029

Villa I, Gracia ML (2004) Estudio hidrogeológico del sinclinal de Estopiñán (Huesca). Confederación Hidrográfica del Ebro, Zaragoza

Walker IR, Smol JP, Engstrom DR, Birks HJB (1991) An assessment of Chironomidae as quantitative indicators of past climatic change. Can J Fish Aquat Sci 48:975–987

Wanner H, Beer J, Bütikofer J, Crowley TJ, Cubasch U, Flückiger J, Goosse H, Grosjean M, Joos F, Kaplan JO, Küttel M, Müller SA, Prentice IC, Solomina O, Stocker

TF, Tarasov P, Wagner M, Widmann M (2008) Mid- to late holocene climate change: an overview. Quat Sci Rev 27:1791–1828. doi:10.1016/j.quascirev.2008.06.013

Weninger B, Jöris O (2004) Glacial radiocarbon calibration. The CalPal program. In: Higham T, Ramsey CB, Owen C (eds) Radiocarbon and archaeology fourth international symposium, Oxford 2002

Wiederholm T (1983) Chironomidae of the Holarctic region. Keys and diagnoses. Part I. Larvae. Entomol Scand Suppl 19:1–457

Witak M, Jankowska D (2005) The Vistula Lagoon evolution based on diatom records. Baltica 18:68–76

Witkowski A, Lange-Betarlot H, Metzeltin D (2000) Diatom flora of marine coasts. In: Lange-Bertalot H (ed) Iconographia diatomologica, p 925

Wolfe AP, Baron JS, Cornett RJ (2001) Anthropogenic nitrogen deposition induces rapid ecological changes in alpine lakes of the Colorado Front Range (USA). J Paleolimnol 25:1–7. doi:10.1023/A:1008129509322

Wunsam S, Schmidt R, Klee R (1995) Cyclotella-taxa (Bacillariophyceae) in lakes of the Alpine region and their relationship to environmental variables. Aquat Sci 57:360–386. doi:10.1007/BF00878399

Zeebe RE (1999) An explanation of the effect of seawater carbonate concentration on foraminiferal oxygen isotopes. Geochim Cosmochim Acta 63:2001–2007. doi:10.1016/S0016-7037(99)00091-5